

Influence of atmospheric deposition on biogeochemical cycles in an oligotrophic ocean system

France Van Wambeke¹, Vincent Taillandier², Karine Desboeufs³, Elvira Pulido-Villena¹, Julie Dinasquet^{4,5}, Anja Engel⁶, Emilio Marañón⁷, Céline Ridame⁸, Cécile Guieu²

5

¹ Aix-Marseille Université, CNRS/INSU, Université de Toulon, IRD, Mediterranean Institute of Oceanography (MIO) UM 110, 13288, Marseille, France

² CNRS, Sorbonne Université, Laboratoire d'Océanographie de Villefranche (LOV), UMR7093, 06230 Villefranche-sur-Mer, France

10 ³ LISA, UMR CNRS 7583, Université Paris-Est-Créteil, Université de Paris, Institut Pierre Simon Laplace (IPSL), Créteil, France

⁴ Sorbonne Universités, Laboratoire d'Océanographie Microbienne (LOMIC), Observatoire Océanologique, 66650, Banyuls/mer, France

⁵ Marine Biology Research Division, Scripps Institution of Oceanography, UCSD, La Jolla, USA

15 ⁶ GEOMAR – Helmholtz-Centre for Ocean Research, Kiel, Germany

⁷ Department of Ecology and Animal Biology, Universidade de Vigo, 36310 Vigo, Spain

⁸ Sorbonne University/CNRS/IRD/MNHN, LOCEAN: Laboratoire d'Océanographie et du Climat: Expérimentation et Approches Numériques, UMR 7159, 4 Place Jussieu – 75252 Paris Cedex 05, France

Correspondence to: France Van Wambeke (france.van-wambeke@mio.osupytheas.fr) and
20 Cécile Guieu (guieu@imev-mer.fr)

Abstract.

The surface mixed layer (ML) in the Mediterranean Sea is a well stratified domain characterized by low macro-nutrients and low chlorophyll content, for almost 6 months of the year. In this study we characterize the biogeochemical cycling of nitrogen (N) in the ML by 25 analysing simultaneous *in situ* measurements of atmospheric deposition, nutrients in seawater, hydrological conditions, primary production, heterotrophic prokaryotic production, N₂ fixation and leucine aminopeptidase activity. Dry deposition was continuously measured across the central and western open Mediterranean Sea and two wet deposition events were sampled, one in the Ionian Sea and one in the Algerian Basin. Along the transect, N budgets 30 were computed to compare the sources and sinks of N in the mixed layer. *In situ* leucine aminopeptidase activity made up 14 to 66 % of the heterotrophic prokaryotic N demand, and the N₂ fixation rate represented 1 to 4.5 % of the phytoplankton N demand. Dry atmospheric

deposition of inorganic nitrogen, estimated from dry deposition of (nitrate and ammonium) in aerosols, was higher than the N₂ fixation rates in the ML (on average 4.8-fold). The dry atmospheric input of inorganic N represented a highly variable proportion of biological N demand in the ML among the stations, 10 - 82% for heterotrophic prokaryotes and 1-30% for phytoplankton. As some sites were visited during several days the evolution of biogeochemical properties in the ML and within the nutrient-depleted layers could be followed. At the Algerian Basin site, the biogeochemical consequences of a wet dust deposition event were monitored by a high frequency sampling of CTD casts. Notably just after the rain, nitrate was higher in the ML than in the nutrient depleted layer below. Estimates of nutrient transfer from the ML into the nutrient depleted layer could explain up to a 1/3 of the nitrate loss from the ML. Phytoplankton did not benefit directly from the atmospheric inputs into the ML, probably due to high competition with heterotrophic prokaryotes, also limited by N and phosphorus (P) availability at the time of this study. Primary producers decreased their production after the rain, they recovered their initial state of activity after a 2-day lag in the vicinity of the deep chlorophyll maximum layer.

1. Introduction

The Mediterranean Sea (MS) is a semi-enclosed basin characterized by active ventilation and short residence times of the newly formed waters, due to its own thermohaline circulation (Mermex Group, 2011). In terms of biogeochemistry, the MS is characterized by a long summer stratification period, a west-to-east gradient of increasing oligotrophy, and a deficit in phosphorus (P) compared to nitrogen (Mermex Group, 2011). The last feature is confirmed by a deep N/P ratio for inorganic nutrients higher than the Redfield ratio that increases toward the east (Krom et al., 2004).

The relationship between photoautotrophic unicellular organisms and heterotrophic prokaryotes (competition or commensalism) is affected by the balance of light and nutrients as well as possible inputs of organic matter from river runoff or atmospheric deposition.

Phytoplankton generally experience P, or N limitation, or both (Thingstad et al., 2005 ; Tanaka et al., 2011, Richon et al., 2018), whereas heterotrophic prokaryotes are usually P limited, or P and organic carbon co-limited (Sala et al., 2002, Van Wambeke et al., 2002, Céa et al., 2014).

The MS continuously receives anthropogenic aerosols, originating from industrial and domestic activities from around the basin and from other parts of Europe, along with pulsed

natural inputs from the Sahara. It is thus a natural LNLC study area, well adapted to investigate the role of ocean–atmosphere exchanges of particles and gases on marine biogeochemical cycles. Recent studies describe annual records of atmospheric deposition of trace metals and inorganic macronutrients (N, P) obtained at several locations around the MS
70 (Markaki et al., 2010; Guieu and Ridame, in press; Desboeufs, in press). All records show pulsed and highly variable atmospheric inputs. Recent models and observations show that atmospheric deposition of organic matter (OM) is also highly variable and that their annual inputs are of the same order of magnitude as river inputs (Djaoudi et al., 2017, Kanakidou et al., 2018; Kanakidou et al., 2020; Galetti et al., 2020). Moreover, the sum of atmospheric
75 inputs of nitrate, ammonium and soluble organic nitrogen has been shown to be equivalent or higher than those of N_2 fixation rates (Sandroni et al., 2007), although inorganic atmospheric N inputs alone may also be higher than N_2 fixation rates (Bonnet et al., 2011).

Aerosol amendments in bottles, minicosms or mesocosms have been widely used to study trophic transfer and potential export, as they allow natural communities to be studied under
80 controlled conditions (i.e. Guieu et al., 2010; Herut et al., 2016; Mescioglu et al., 2019). Both diversity and functioning of various biological compartments are impacted by aerosol additions in different waters tested in the MS (Guieu and Ridame, in press, and Figure 3 therein). Differences in the biological responses have been observed, depending on the mode of deposition simulated (wet or dry), the type of aerosols used (natural or anthropogenic) and
85 the *in situ* biogeochemical conditions at the time of the experiment (Guieu and Ridame, in press).

Organic carbon from aerosols is partly soluble, and this soluble fraction is partly available to marine heterotrophic prokaryotes (Djaoudi et al., 2020). Heterotrophic prokaryotes have the metabolic capacity to respond quickly to aerosol deposition through growth and changes in
90 community composition (Rahav et al., 2016; Pulido-Villena et al., 2008; 2014), while the phytoplankton community responds more slowly or not at all (Guieu and Ridame, in press, and reference therein).

Owing to the intrinsic experimental limitations, which vary depending on the size and design of enclosures (i.e. the omission of higher trophic levels, absence of turbulent mixing so
95 limiting exchanges by diffusion, and wall effects) such experiments cannot, however, fully simulate *in situ* conditions (Guieu and Ridame, in press). Thus, *in situ* observations are required to understand the consequences of aerosol deposition on biogeochemical cycling in the world's ocean. Such *in situ* studies are scarce and require dedicated, high-frequency

100 sampling to follow the effects of deposition on the biogeochemical processes while taking
into account the water column dynamics as recently emphasized in cases studies (Pulido-
Villena et al., 2008 and Rahav et al., 2016).

105 Hence, there is a need for sampling surveys with adaptive strategies to follow aerosol
deposition events *in situ* and their impacts on biogeochemical processes, especially in the
open waters of the stratified and nutrient limited MS. The objectives of the PEACTIME
project were to study fundamental processes and their interactions at the ocean–atmosphere
interface following atmospheric deposition (especially of Saharan dust) in the Mediterranean
Sea, and how these processes impact the functioning of the pelagic ecosystem (Guieu et al.,
2020).

110 As atmospheric deposition affects primarily the surface mixed layer (ML), the present study
focuses on the upper part of the nutrient depleted layer that extends down to the nutriclines (as
defined by Du et al., 2017). During the stratification period, concentrations of nitrate and
phosphate inside the ML are often below the detection limits of standard methods. However,
nanomolar concentrations of nitrate (and phosphate) can now be assessed accurately through
the Long Waveguide Capillary Cell (LWCC) technique (Zhang and Chi, 2002), which permits
115 the measurement of fine gradients inside nutrient depleted layers of the MS (Djaoudi et al.,
2018).

120 The aims of the present study were to assess the impact of atmospheric nutrient deposition on
biogeochemical processes and fluxes in the open sea during the PEACTIME cruise in the MS.
For this i) we estimated nanomolar variations of nitrate concentration in the surface mixed
layer (ML) under variable inputs of dry and wet aerosol deposition and ii) we compared the
aerosol-derived N inputs to the ML with biological activities: primary production,
heterotrophic prokaryotic production, N₂ fixation and ectoenzymatic (leucine aminopeptidase)
activity. We studied the N budgets along a zonal transect that includes 13 stations crossing the
125 Algerian Basin, Tyrrhenian Sea and the Ionian Sea where dry atmospheric deposition was
continuously measured on board together with seawater biogeochemical, biological and
physical characteristics. We finally focused on a wet deposition event that occurred in the
western Algerian Basin, where we investigated the evolution of biogeochemical fluxes of
both N and P and microbial activities through the high frequency sampling.

130 **2. Materials and Methods**

2.1 Sampling strategy and measured parameters

The PEACETIME cruise (doi.org/10.17600/15000900) was conducted in the Mediterranean Sea, from May to June 2017, along a transect extending from the Western Basin to the center of the Ionian Sea (Fig. 1). For details on the cruise strategy, see Guieu et al. (2020). Short duration stations (< 8 h, 10 stations named ST1 to ST10, Fig. 1) and long duration sites (5 days, 3 sites named TYR, ION and FAST) were occupied. Chemical composition of aerosols was quantified by continuous sampling along the whole transect. In addition, two rain events were sampled (Desboeufs et al., this issue, in prep.), one on the 29th of May at ION site, and a second one, a dust wet deposition event, at FAST site on the 5th of June.

At least 3 CTD casts were conducted at each short station. One cast focused on the epipelagic layer (0-250 m), another on the whole water column. Two were carried out with a standard, CTD rosette equipped with 24 Niskin bottles (12 L), and a Sea-Bird SBE9 underwater unit with pressure, temperature (SBE3), conductivity (SBE4), chlorophyll fluorescence (Chelsea Aquatracka) and oxygen (SBE43) sensors. A third cast, from the surface to the bottom of the water column was carried out under trace metal clean conditions using instrumental package including a titanium rosette (hereafter TMC-rosette) mounted on a Kevlar cable and equipped with Go-Flo bottles that were sampled in a dedicated clean lab container. The long duration sites were abbreviated as TYR (situated in the center of the Tyrrhenian Basin), ION (in the center of the Ionian Basin) and FAST (in the western Algerian Basin). These 3 sites were selected based on satellite imagery, altimetry and Lagrangian diagnostics as well as forecasted rain events (Guieu et al., 2020). At these sites, repeated casts were performed over at least 4 days with alternating CTD- and TMC- rosettes (Table 1).The succession of CTD casts at the FAST site is numbered in days relative to a rain event sampled on board the ship. The first cast of the series was sampled 2.3 days before the rain event, and the last 2 days after. The FAST site was revisited following the study at ST10 (3.8 days after the rain event).

Primary production (PP), prokaryotic heterotrophic production (BP), heterotrophic prokaryotic abundances (hprok), ectoenzymatic activities (leucine aminopeptidase (LAP) and alkaline phosphatase (AP)), were determined on water samples collected with the standard CTD-rosette. Dissolved inorganic nutrients, dissolved organic nitrogen (DON) and phosphorus (DOP) were measured on water samples collected using the TMC-rosette. LAP and AP were determined from two layers in the epipelagic waters (5 m depth and deep chlorophyll maximum (DCM)) at the short stations and at the ION and TYR sites In addition, LAP and AP were determined at 4 depths between 0 and 20 m for 4 profiles at FAST site, to determine the variability within the ML.

2.2 Analytical methods and fluxes calculations

2.2.1 Nutrients in the atmosphere

Total suspended aerosol particles (TSP inlet) were collected continuously throughout the campaign for dry deposition estimations. Aerosol sampling was carried out using filtration units on adapted membranes for off-line chemical analysis (Tovar-Sanchez et al., 2020).

Simultaneously, water soluble fraction of the aerosols was sampled continuously, using a Particle-into-Liquid-Sampler (PILS, Orsini et al., 2003). Moreover, two wet deposition events were sampled, one at the ION site, one at the FAST site using rain collectors with on-line filtration (porosity 0.2 μm) (details in Desbeoufs et al., this issue, in prep)

175 Nitrate and ammonium concentrations in the aerosols, abbreviated in the text as NO₃ and NH₄ respectively, were analyzed continuously on board from May 13th, using PILS sampling coupled on-line with double way ion chromatography (PILS-IC, Metrohm, model 850

Professional IC with Metrosep A Supp 7 column for anion measurements and Metrosep C4 column for cation measurements). The temporal resolution for PILS-IC analysis was 70 min

180 for anions and 32 min for cations. Dissolved Inorganic Nitrogen (DIN) fluxes released by dry deposition were estimated by multiplying NO₃ and NH₄ obtained through PILS-IC measurements (nitrite concentrations were under analytical detection limits) by the dry

settling velocities of N-bearing aerosols, i.e 0.21 and 1 cm s^{-1} for NH₄ and NO₃, respectively (Kouvarakis et al., 2001). Mean NO₃ and NH₄ concentrations were calculated from the PILS-

185 IC data measured (1) during the occupation of each short station lasting between 0.13 and 0.66 days (with on average 5 measurements for NO₃ and 11 measurements for NH₄), and (2) between two successive casts at the sites with a time lag between 0.4 and 1.21 days (with on average 15 measurements for NO₃ and about 30 for NH₄). At ST1, NH₄ and NO₃

concentrations were obtained using IC analyses following water extraction from aerosol filter 190 sampling as the PILS-IC was not operational.

Total dissolved phosphate (TDP) concentrations were estimated from soluble P concentrations extracted from particulate aerosols collected on filters after ultrapure water extraction HR-ICP-MS analysis (Neptune Plus, Thermo Scientific TM) (Fu et al., this issue, in prep) since it was generally below the detection limits of the PILS-IC technique. The

195 frequency of TDP analysis was therefore less than for NO₃ and NH₄ (0.28 -1.15 days depending on the stations). At the ION, TYR and FAST sites, filters collected aerosols at different periods including each CTD cast, when possible.

Atmospheric deposition of soluble P was estimated by multiplying the TDP concentration by a dry settling velocity of 1 cm s^{-1} , except at the FAST site where 3 cm s^{-1} was used as this
200 value is better adapted for lithogenic particles (Izquierdo et al., 2012). The dissolved fraction and solution from digestion (Heimburger et al., 2012) of particulate fractions in the filters were analysed by ICP-AES (Inductively Coupled Plasma Atomic Emission Spectrometry, Spectro ARCOS Ametek®). The speciation organic/inorganic of TDP was determined from ICP-MS and IC analysis. DOP was estimated from the difference between TDP, obtained by
205 ICP-MS, and DIP, obtained by ion chromatography.

In the rain samples NO₃, NH₄ and dissolved inorganic phosphorus (DIP) were also determined using ion chromatography following recovery of the dissolved fraction.. Total particulate P (TPP) and dissolved organic P (DOP) were also measured in the rain samples following a similar protocol used for atmospheric dust (described above).The wet deposition
210 fluxes of dust dissolved nutrients and particulate fractions were estimated from the measured concentrations in the rain sample, multiplied by total precipitation.

Total precipitation was taken from the total hourly precipitation accumulated during the rain event over the region from the ERA5 hourly data reanalysis (Hersbach et al., 2018). In order to incorporate the regional variability of rainfall, the total precipitation was taken from the
215 total hourly precipitation over a domain whose center is the ship and whose radius measures 110 km using the ERA5 hourly data reanalysis (Hersbach et al., 2018). ERA 5 data are available on regular latitude-longitude grids at $0.25^\circ \times 0.25^\circ$ resolution (Desboeufs et al., in prep, Table 3). Cumulative precipitation was obtained by considering the value at the center of each grid point over the domain.

220

2.2.2 Nutrients in the water column

Seawater samples for standard nutrient analysis were filtered online ($< 0.2 \mu\text{m}$, Sartorius Sartrobran-P-capsule with a $0.45 \mu\text{m}$ prefilter and a $0.2 \mu\text{m}$ final filter) directly from the Go-FLo bottles (TMC-rosette). Samples collected in acid-washed polyethylene bottles were
225 immediately analyzed on board. Micromolar concentrations of nitrate + nitrite (NO_x) and DIP were determined using a segmented flow analyzer (AAIII HR SealAnalytical©) following Aminot and Kérouel (2007) with a limit of quantification (calculated as ten times the standard deviation of ten measurements of the blank) of $0.050 \mu\text{M}$ for NO_x and $0.020 \mu\text{M}$ for DIP. Samples for the determination of nanomolar concentrations of dissolved nutrients were
230 collected in HDPE bottles previously cleaned with supra-pure HCl. For NO_x (primarily NO₃

as the nitrite fraction was mostly negligible), samples were acidified to pH 1 inside the clean container and analyzed back in the laboratory using a spectrometric method in the visible (540 nm), with a 1 m LWCC (Louis et al., 2015). The detection limit was 6 nM, the limit of quantification was 9 nM and the reproducibility was 8.5%. DIP was analyzed immediately 235 after sampling using the LWCC method after Pulido-Villena et al. (2010), with a detection limit of 1 nM (Pulido-Villena et al., 2021). Total dissolved phosphorus (TDP) and nitrogen (TDN) were measured using the segmented flow analyzer technique after high-temperature (120 °C) persulfate wet oxidation mineralization (Pujo-Pay and Raimbault, 1994). DOP (DON) was obtained as the difference between TDP (TDN) and DIP (NOx). Labile DOP (L-DOP) was estimated as 31% of the DOP values (Pulido-Villena et al., 2021).
240 Total hydrolysable amino acids (TAAs) were determined as described in detail in Van Wambeke et al. (2021). Briefly 1 ml of sample was hydrolyzed at 100°C for 20 h with 1 ml of 30% HCl and then neutralized by acid evaporation. Samples were analyzed by high performance liquid chromatography in duplicate according to Dittmar et al. (2009) protocols.
245

2.2.3 Biological stocks and fluxes in the epipelagic waters

Flow cytometry was used for the enumeration of autotrophic prokaryotic and eukaryotic cells, heterotrophic prokaryotes (hprok) and heterotrophic nanoflagellates (HNF). Water samples (4.5 mL) were fixed with glutaraldehyde grade I 25% (1% final concentration), flash frozen 250 and stored at -80 °C until analysis. Counts were performed on a FACSCanto II flow cytometer (Becton Dickinson). The separation of different autotrophic populations was based on their scattering and fluorescence signals according to Marie et al. (2000). For the enumeration of hprok (Gasol and Del Giorgio, 2000), cells were stained with SYBR Green I (Invitrogen – Molecular Probes). HNF staining was performed with SYBR Green I as 255 described in Christaki et al. (2011). All cell abundances were determined from the flow rate, which was calibrated with TruCount beads (BD biosciences).

Particulate primary production (PP) was determined at 6 layers from the shallow CTD casts (0-250 m) sampled before sun rise. Samples were inoculated with ¹⁴C-bicarbonate and 260 incubated in on-deck incubators kept at in situ temperature by flowing surface seawater and equipped with various blue screens to simulate different irradiance levels. After 24 h-incubations, samples were filtered through 0.2 polycarbonate filters and treated for liquid scintillation measurement as described in detail in Marañón et al. (2021). A temperature

correction was applied as explained in Marañón et al. (2021). N₂ fixation rates (N2fix) were determined as described in Ridame et al. (2011) using 2.3 L of unfiltered seawater collected 265 in acid-washed polycarbonate bottles and enriched with ¹⁵N₂ gas (99 atom% 15N) to obtain a final enrichment of about 10 atom% excess. 24 h-incubations for N2fix were conducted under the same temperature and irradiance as the corresponding PP incubations.

To calculate heterotrophic prokaryotic production (BP) samples collected in the epipelagic 270 layers (0-250 m) were incubated with tritiated leucine using the microcentrifuge technique as detailed in Van Wambeke et al. (2021). We used the empirical conversion factor of 1.5 ng C per pmol of incorporated leucine according to Kirchman (1993). Isotope dilution was negligible under these saturating concentrations as periodically checked with concentration 275 kinetics. As we only used 2 on board temperature controlled dark-incubators, a temperature correction was applied as explained in Van Wambeke et al. (2021). Ectoenzymatic activities were measured fluorometrically, using the fluorogenic model substrates L-leucine-7-amido-4-methyl-coumarin (Leu-MCA) and 4-methylumbelliferyl-phosphate (MUF-P) to track 280 aminopeptidase (LAP) and alkaline phosphatase (AP) activity, respectively, as described in Van Wambeke et al. (2021). Briefly, the release of MCA from Leu-MCA and MUF from MUF-P were followed by measuring the increase of fluorescence in the dark (exc/em 380/440 285 nm for MCA and 365/450 nm for MUF, wavelength width 5 nm) in a VARIOSCAN LUX microplate reader. Fluorogenic substrates were added at varying concentrations in 2 ml wells (0.025, 0.05, 0.1, 0.25, 0.5 and 1 μ M) in duplicate. The parameters V_m (maximum hydrolysis velocity) and K_m (Michaelis-Menten constant that reflects enzyme affinity for the substrate) as well as their corresponding errors were estimated by non-linear regression using the 290 Michaelis-Menten equation:

$$V = V_m \times S / (K_m + S)$$

where V is the hydrolysis rate and S the fluorogenic substrate concentration added. LAP and AP *in situ* activities were determined substituting S by TAA and L-DOP in Michaelis-Menten equations, respectively (Van Wambeke et al., 2021; Pulido-Villena et al., 2021).

290

2.3. Vertical nutrient fluxes

In the absence of concomitant turbulence measurements, the mixed layer depth (MLD) can be estimated from density profiles (e.g. de Boyer Montegut et al., 2004; D'Ortenzio et al., 2005). For this study, a MLD was determined at every CTD cast as the depth where the residual

295 mass content (i.e., the vertical integral of the density anomaly relative to surface) was equal to 1 kg m⁻² (Prieur et al., 2020), with an error of estimation of 0.5 m relative to the vertical resolution of the profile (1 m).

In the Mediterranean Sea, the low nutrient availability combined with a shallow mixed layer (ML) lead to the formation of a nutrient depleted layer that extend below the ML. Hereafter, 300 the nutrient depleted layer is referred to 'NDLb' (b for bottom or base) for NO₃ and as PDLb for DIP. This layer vertically extends between the MLD and the nitracline (phosphacline) depth (Fig. 2). The latter interface is estimated by the depth of NO₃ (DIP) depletion, which is the deepest isopycnal at which micromolar NO₃ (DIP) is zero (Kamykowski and Zentara, 1985; Omand and Mahadevan, 2015). The NO₃ (DIP) depletion density is estimated at every 305 discrete profile of micromolar NO₃ (DIP) concentration by the intercept of the regression line reported in a nutrient-density diagram.

There are various mechanisms, dynamical or biological, that can trigger exchanges of nutrients between the ML and NDLb (PDLb). Using the hypothesis of vertical (one-dimensional) regimes, there are two processes of exchange, by diffusion or advection (Du et 310 al., 2017). The flux of nutrient can be expressed as:

$$F_{NO_3} = F_{DIF} + F_{ADV}$$

The diffusive flux F_{DIF} is expressed by the gradient of nutrient concentration times a vertical diffusivity coefficient K_z as:

$$F_{DIF} = K_z \times (NO_3_{ML} - NO_3_{NDLb}) / MLD$$

315 The typical magnitude of K_z in the surface layers of the PEACETIME stations was assessed to be 10⁻⁵ m² s⁻¹, as discussed in Taillardier et al. (2020).

The advective flux F_{ADV} corresponds either to the entrainment of deeper water in the mixed layer due to the erosion of the near-surface pycnocline, or to the detrainment of waters below the mixed layer by restratification, depending on the variations in wind stress and solar 320 heating (Cullen et al., 2002). It is expressed as the variation in the nutrient concentration across the ML times the temporal variation of the MLD, as:

$$F_{ADV} = (NO_3_{ML} - NO_3_{NDLb}) \times dMLD / dt$$

Shallow MLs as the ones observed in this study (10 - 20 m) are primarily influenced by wind bursts that can lead to intermittent variations of the MLD, up to several meters per day (10⁻⁵ m 325 s⁻¹) in the MLD. Resulting advective fluxes provide transient exchanges that are one order of magnitude greater than well-established diffusive fluxes. As a consequence, over the time scale of a significant atmospheric deposition, associated rapid variations of the MLD would

rather promote the input of atmospheric nutrients to be exported below the ML by advection rather than by diffusion. In other terms, using the hypothesis of non-stationary regimes due to 330 rapid changes in atmospheric conditions (that control both the mixing state of the ML and atmospheric nutrient inputs), we assume that vertical advection is the main process of exchange.

At the short stations and sites, the term $\text{NO}_3_{\text{ML}} - \text{NO}_3_{\text{NDLb}}$ can be inferred by the difference 335 between mean nanomolar (LWCC) concentrations within the NDLb and the ML. At short stations, as advective fluxes could not be characterized, only a qualitative assessment of nutrient fluxes across ML is given. When $\text{NO}_3_{\text{ML}} - \text{NO}_3_{\text{NDLb}} < 0$, the NDLb is supplied with NO_3 across the nutricline, and could be then possibly transferred into the ML. This means that nutrients within the ML are impacted by inputs from below. When $\text{NO}_3_{\text{ML}} - \text{NO}_3_{\text{NDLb}} > 0$, the ML is supplied in NO_3 from the atmosphere which is further exported into the NDLb. 340 Vertical distributions of DIP, along the longitudinal transect, are described in detail in a companion paper (Pulido-Villena et al., 2021).

2.4 Budget from the metabolic fluxes

Trapezoidal integration was used to integrate BP, PP and N2fix within the ML. The biological 345 activity at the surface was considered to be equal to that of the first layer sampled (around 5 m depth at the short stations, 1 m depth at the FAST site). When the MLD was not sampled, the volumetric activity at that depth was linearly interpolated between the 2 closest data points above and below the MLD.

We used an approach similar to Hoppe et al. (1993) to compute the *in situ* hydrolysis rates for 350 LAP and AP. We assumed that total amino acids (TAA) could be representative of dissolved proteins. *In situ* hydrolysis rates of LAP and AP were determined using molar concentrations of TAA and L-DOP, respectively and used as the substrate concentration in the Michaelis-Menten kinetics. For LAP, the transformation of *in situ* rates expressed in nmol TAA hydrolyzed $\text{L}^{-1} \text{h}^{-1}$ were then transformed into nitrogen units using N per mole TAA, as the 355 molar distributions of TAA were available. Integrated *in situ* LAP hydrolysis rates were calculated assuming the Michaelis-Menten parameters V_m and K_m obtained at a 5 m depth to be representative of the whole ML. Thus an average *in situ* volumetric LAP flux in the ML was obtained by combining the average TAA concentrations in the ML with these kinetic parameters, and multiplying this volumetric rate by the MLD. Daily BP, AP and LAP 360 integrated activities were calculated from hourly rates $\times 24$. Assuming no direct excretion of

either nitrogen or phosphorus, the quota C/N and C/P of cell demand is equivalent to the cell biomass quotas. We used molar C/N ratios derived from Moreno and Martiny (2018) (range 6-8, mean 7) for phytoplankton and from Nagata et al. (1986) for heterotrophic prokaryotes (range 6.2-8.4, mean 7.3). C/P of sorted cells (cyanobacteria, picophytoeukaryotes) in P depleted conditions ranged from 107 to 161 (Martiny et al., 2013), and we considered a mean of 130 for phytoplankton. A value of 100 was used for heterotrophic prokaryotes (Godwin and Cotner, 2015).

3. Results

370

3.1 Nutrient patterns and biological fluxes along the PEACETIME transect

The MLD ranged between 7 m at ST9 and 21 m at ST1 (Table S1, Fig. 3). The nitracline was shallow in the Provençal Basin (50 – 60 m), dropping to 70 m in the Eastern Algerian and Tyrrhenian Seas; becoming deeper in the Western Algerian and Ionian Seas (80 - 90 m, Table

375

S1). Mean NO₃ concentrations in the NDLb ranged from the quantification limit (9 nM) to 116 nM (Table S1, Fig. 4). In the ML, mean NO₃ concentrations ranged from 9 to 135 nM. For the ‘group 1’ stations (see Table S1), NO₃ concentrations were low (below 50 nM) both within the ML and the NDLb, with weak gradient between the two layers. For the ‘group 2’ stations, NO₃ concentrations were moderate (50 - 80 nM) both within the ML and the NDLb 380 but still exhibiting a small difference between the two layers, indicating again no significant instantaneous exchanges. For ‘group 3’, higher NO₃ concentrations were measured in both the ML and the NDLb (> 80 nM) but the small positive differences (< 20 nM) between the two layers still indicate weak or negligible exchanges between the two layers. For ‘group 4’, high and moderate NO₃ concentrations were measured within the ML and NDLb,

385

respectively, with a large positive difference (> 20 nM) between the layers. This indicates the presence of a gradient from the ML to the NDLb.

At 5 m depth, the leucine aminopeptidase (LAP) kinetic parameter V_m ranged from 0.21 to 0.56 nmol MCA-leu hydrolyzed l⁻¹ h⁻¹, and K_m LAP ranged from 0.12 to 1.29 μM. The mean TAA within the ML ranged from 0.17 to 0.28 μM. The mean *in situ* LAP hydrolysis rate 390 within the ML, derived from these 3 series of parameters, ranged from 0.07 to 0.29 nmol N l⁻¹ h⁻¹ (results not shown but detailed in Van Wambeke et al., 2021).

The vertical distributions of PP and BP for the short stations are described in Marañon et al. (2021). Briefly, PP exhibited a deep maximum close to the DCM depth or slightly above

whereas vertical distribution of BP generally showed 2 maxima, one within the mixed layer, and a second close to the DCM. Integrated PP (Table 1, Table S2) ranged from 138 (TYR17 May) to 284 (SD1) $\text{mg C m}^{-2} \text{ d}^{-1}$. Integrated BP (0-200 m) ranged from 44 (ION27May) to 113 (FAST+0.53) $\text{mg C m}^{-2} \text{ d}^{-1}$. Overall, at the time of the PEACETIME cruise, the transect exhibited the classical west-east gradient of increasing oligotrophy detected by ocean colour (see Fig. 8 in Guieu et al., 2020),

400

3.2 N budgets and fluxes at short stations

Biological rates (all expressed in N units) within the ML at the short stations were compared. (Table 2). Phytoplankton N demand (phytoN demand) was the greatest rate, followed by heterotrophic prokaryotic N demand (hprokN demand). On average, phytoN demand was 2.9 (range 1.5 – 8.1) times greater than that of hprokN. LAP hydrolysis rates represented between 405 14 and 66 % of the hprokN demand (mean \pm sd : $37\% \pm 19\%$), N_2 fixation rates represented between 1 to 4.5% of the phytoN demand ($2.6\% \pm 1.3\%$) and 3 to 11% of the hprok N demand ($6.4\% \pm 2.4\%$). N_2 fixation rates integrated over the ML correlated slightly better with hprokN demand ($r = 0.75$) than with phytoN demand ($r = 0.66$).
410 Dissolved inorganic N (DIN=NO₃+NH₄) solubilized from dry atmospheric deposition ranged from 17 to 40 $\mu\text{mol N m}^{-2} \text{ d}^{-1}$ of which 79% on average were NO₃ (Table 2). This new DIN input was similar or higher than N_2 fixation rates within the ML (from 1.3 to 11 fold, mean 4.8-fold). On average, the new DIN from dry deposition represented 27% of the hprokN demand (range 10-82%) and 11% of the phytoN demand (range 1-30%) within the ML.

415

3.3 Biogeochemical evolution at the ION site

The ION site was occupied May 25 to 29. Rain events in the vicinity of the ship were observed on May 26 and May 29 (Desboeufs et al., this issue, in prep). On the May 29 the 420 rain event was associated with a rain front covering more than 5 000 km^2 . A rain sample could be taken on board between 5:08 and 6:00 (local time), i.e. just 3 hours before the last CTD cast. The chemical composition of the rain indicated an anthropogenic background influence (Desboeufs et al., this issue, in prep.).

TDP solubilized from dry atmospheric deposition decreased from 268 $\text{nmol P m}^{-2} \text{ d}^{-1}$ May 25 425 -26 to 124 $\text{nmol P m}^{-2} \text{ d}^{-1}$ May 27-28). DIN fluxes from dry atmospheric deposition averaged $29 \pm 4 \mu\text{mol N m}^{-2} \text{ d}^{-1}$ with small variability during the occupation of the site (Table S2). The

molar ratio DIN/DIP in the rain was 208 and DOP represented 60% of the total dissolved P (Table 3).

CTD casts, dedicated to biogeochemical studies, were taken each 24 h for biological fluxes or 430 48 h for DIP and NO₃. Thus the time sequence for nutrients in the water column at ION is given for only by three profiles. The first profile (May 25 before rain events in the area) is 'flat', corresponding to smooth weather conditions and a shallow ML with low and homogeneous concentrations of NO₃ in the ML and the NDLb (Fig. 4). Shortly after, there 435 was an atmospheric depression: some rain events were observed in the area on May 26 but not on board and the ML started to deepen 13 h before the second cast with nutrient sampling (on May 27). This cast reflected high NO₃ in the ML (Fig. 3). The mixing should have set up a homogeneous ML, but wind conditions rose to 20 kt just at the time of the cast (Fig. 3). The interval between the second and the third cast sampling nutrients (May 29, cast done 3 hours after the rain sampled on board) was marked by a slight relaxation of weather depression, and 440 a deepening of the ML down to 20 m. This cast reflected a NO₃ decrease in both the ML and NDLb, but with NO₃ concentrations higher in ML. The calculation of vertical advective fluxes between the two layers showed a downward flux in the first interval May 25-27 (Fig. 4, Table S1) and an upward flux in the second interval (May 27-29). Due to the lack of high frequency sampling, it was also particularly difficult to assess the 445 direct time evolution effects of dry atmospheric deposition at the ION site. Nevertheless, it was clear from the casts sampled on the May 27 and 29, that this site was characteristic of group 4 (i.e. higher NO₃ concentrations in the ML than in the NDLb), suggesting recent inputs from the atmosphere. Ectoenzymatic activities were only sampled on May 25. Vm of LAP at 5 m (0.22 nmol N l⁻¹ h⁻¹) was one of the lowest values recorded during the cruise 450 whilst Vm of AP was the highest (5.6 nmol P l⁻¹ h⁻¹). PP integrated over the euphotic zone increased slightly from 188 to 226 mg C m⁻² d⁻¹ (Table S2), but due to changes in the MLD at the ION site (range 11-21 m) this trend was not visible when integrating PP over the ML. Integrated over the ML, BP increased slightly, from 7.5 to 10.3 mg C m⁻² d⁻¹ between May 25 455 and May 29, and indicated that hprok benefited more from the atmospheric inputs than the autotrophs as PP decreased at 5m depth (Fig. S1, Table S2). The profiles of hprok and *Synechococcus* abundances showed no particular trend with time, with higher variations within the DCM (Fig. S1).

3.4 N budgets and fluxes at the FAST site

460 During the occupation of the FAST site, two rains episodes took place: the evening of June 2-
night of June 3 and the early morning of June 5 (Tovar-Sanchez et al., 2020). The rain radar
data indicated the presence of a rain front with patchy, numerous and intense rain events
occurring over a large area surrounding the ship's location. These two episodes coincided
with a dust plume transported in altitude (between 1 and 4 km) and resulted in wet deposition
465 of dust (Desboeufs et al., this issue, in prep.). A rain sample was collected on board on June
5th (between 02:36 and 03:04, local time) and was associated with a dust wet deposition flux
~ 40 mg m⁻². The DIN/DIP ratio in the rain reached 480 (Table 3). After the rain, daily fluxes
of DIN solubilized from dry aerosol deposition strongly decreased from 45 to 9.8 µmol N m⁻²
d⁻¹ between June 4 and 5.

470 The beginning of the water column sampling at FAST site (-2.3; -1.5; -0.25) was marked by
moderate and similar decreases in NO₃ concentration within the ML and NDLb. Integrated
stocks of NO₃ within the ML (Table S2) reflected slight changes of MLD (from 14 to 10 m
during this time interval). On June 5th, the rain event (Table 3) was associated with a strong
475 wind burst and an abrupt mixing. The comparison between NO₃ concentrations from two
casts, sampled 6 h before and 6 h after the rain, (FAST-0.25 and FAST+0.24), showed a clear
N enrichment of the ML as mean NO₃ increased from 56 to 93 nM and NO₃ integrated stocks
increased by 888 µmol N m⁻² (Fig. 3, Table S2). There was also clear difference in the mean
NO₃ concentrations between ML and NDLb (93 ± 15 vs 51 ± 7 nM, respectively). This is the
480 highest NO₃ difference observed during the cruise between these 2 layers (Fig. 4), confirming
that this ML enrichment could not be attributed to inputs from below. The relaxation of this
wind burst was progressive, with a continuous deepening of the ML (Table S1). The export of
the atmospheric NO₃ into the NDLb was maximal after the rain event (FAST+0.24). At the
end of the site occupation period (FAST+3.8) high NO₃ concentrations (mean 135 nM) were
485 measured again within the ML.

DIP concentration dynamics were different from those of NO₃, with similar DIP integrated
stocks within the ML being measured 6 h before and 6 h after the rain (136 µmol m⁻²). From
then on, DIP stocks progressively increased reaching a maximum (281 µmol P m⁻²) one day
after the rain (FAST+1).

490 Immediately after the rain, integrated PP (euphotic zone) decreased from 274 mg C m⁻² d⁻¹
(FAST-0.9) to 164 mg C m⁻² d⁻¹ (FAST+0.07) and continued to decrease the following day. It
was only 3.8 days after the rain that the initial values (before the rain) of integrated PP could

be observed again (Table S2). Such variations were mostly due to changes in volumetric rates within the DCM depth (Fig. S2), as the activity did not change significantly within the ML
495 (28-33 mg C m⁻² d⁻¹, Fig. S2, Fig. 5). Integrated BP over 0-200 m showed the opposite trend to that of PP and tended to increase after the rain (from 86 ± 3 mg C m⁻² d⁻¹ (n = 4) before, and up to 113 mg C m⁻² d⁻¹ (FAST+0.5) after (Table S2)). Although modest, this increasing trend was also visible when integrating BP only over the ML (12-15 before; 15-19 mg C m⁻² d⁻¹ after). The abundances of picophytoplankton groups were mostly varying in the vicinity of the
500 DCM depth with peaks occurring 1-2 days after the rain (grey profiles, Fig S3), in particular for prokaryotes (*Prochlorococcus*, *Synechococcus*). Heterotrophic prokaryotes and nanoflagellate abundances slightly increased within the DCM depth after the rain.

4. Discussion

505 The specific context of the oceanographic survey constrained the temporal and spatial coverage of our analysis, as the biogeochemical responses to a rain event were investigated over a few days (3 - 5), and tens of km (40 - 50). Their evolution was restricted to the vertical dimension, integrating lateral exchanges by horizontal diffusion or local advection that
510 occurred over the prescribed space and time scales. In the vertical dimension, exchanges of nutrients across the ML were controlled by advection due to rapidly changing conditions (MLD fluctuations along with nutrient inputs from the atmosphere) rather than to diffusion between stationary pools. Four groups of stations, corresponding to different stages of ML enrichment and relaxation, due to the nutrient inputs from single rain events, have been
515 characterized based on the differences in NO₃ concentration between ML and NDLb (see section 2.4). As shown in Fig. 4, this succession of stages is in agreement with the NO₃ fluxes from above and below the ML. Moreover, they provide a temporal scaling of the oceanic response to atmospheric deposition, with a quasi-instantaneous change at the time of the rain event and a 2-day relaxation period to recover to pre-event conditions
520 In this context, we will i) discuss the nitrogen budget within the ML at the short stations considered as a ‘snapshot’, and ii) analyze in detail, using a time series of CTD casts, the biogeochemical changes within the ML and the NDLb following the atmospheric wet deposition event at the FAST site, discussing the possible modes of transfer of nutrients between these 2 layers.

4.1 A snapshot of biological fluxes in the ML and their link to new DIN from atmospheric dry deposition

The dependence of hprok on nutrients rather than on labile organic carbon during stratification conditions is not uncommon in the MS (Van Wambeke et al., 2002, Céa et al, 530 Sala et al., 2002) and has also been shown during PEACETIME cruise (P, or N,P colimitation, Fig. S4). Hprok have an advantage due to their small cell size and their kinetic systems which are adapted to extremely low concentrations of nutrients (for example for DIP see Talarmin et al., 2015). Under such conditions of limitation, hprok will react rapidly to new phosphorus and nitrogen inputs, coming from atmospheric deposition. During an 535 artificial *in situ* DIP enrichment experiment in the Eastern Mediterranean, P rapidly circulated through hprok and heterotrophic ciliates, while the phytoplankton was not directly linked to this 'bypass' process (Thingstad et al., 2005). Bioassays conducted in the tropical Atlantic Ocean have also shown that hprok respond more strongly than phytoplankton to nutrients from Saharan aerosols (Marañón et al. 2010), a pattern that has been confirmed in a meta- 540 analysis of dust addition experiments (Guieu et al., 2014; Guieu and Ridame, in press; Gazeau et al., 2021).

We considered hprokN demand together with phytoN demand and compared it to autochthonous (DON hydrolysis by ectoenzymatic activity) and allochthonous (atmospheric 545 deposition) sources. To the best of our knowledge this is the first time that these fluxes are compared based on their simultaneous quantification at sea. A high variability was observed among the 10 short stations (Table 2). The regeneration of nitrogen through aminopeptidase activity was clearly the primary provider of N to hprok as 14 to 66% (mean \pm sd : 37% \pm 19%) of the hprokN demand could be satisfied by *in situ* LAP activity. Such percentages may 550 be largely biased by the conversion factors from C to N and propagation of errors for the LAP hydrolysis rates and BP rates. However, the C/N ratio of hprok is relatively narrow under large variations of P or N limitation (6.2 to 8.4; Nagata, 1986). Other regeneration sources exist such as direct excretion of NH4 or low molecular weight 555 DON sources with no necessity for hydrolysis prior to uptake (Jumars et al., 1989). For instance, Feliú et al. (2020) calculated that NH4 and DIP excretion by zooplankton would satisfy 25-43% of the phytoN demand and 22-37% of the phytoP demand over the whole euphotic zone. Such percentages suggest that direct excretion by zooplankton along with ectoenzymatic activity provide substantial N for biological activity.

N₂ fixation is also a source of new N that can directly fuel hprok as some diazotrophs are
560 heterotrophic (Delmont et al. 2018, and references therein), or indirectly, as part of the fixed
N₂ that rapidly cycles through hprok (Caffin et al., 2018). Furthermore, it has been observed
that there is a better coupling of N₂fixation rates with BP rather than with PP in the eastern
MS (Rahav et al., 2013b). This was also observed within the ML in this study. Our data
showed that the hypothetical contribution of N₂fixation rates to hprokN demand within the
565 ML was low ($6.4 \pm 2.4\%$) and consistent with the low N₂fixation rates observed in the MS (i.e
Rahav et al., 2013a; Ibello et al., 2010; Ridame et al., 2011; Bonnet et al., 2011). This differs
from other parts of the ocean primarily limited by N but not by P, such as the south eastern
Pacific where N₂ fixation rates are high (Bonnet et al., 2017) and can represent up to 81 % of
the hprokN demand (Van Wambeke et al., 2018).

570 The sum of LAP activity and N₂ fixation were not sufficient to meet hprokN demand (total
contribution between 19 to 73% of HbactN demand). Finally, we examined the source of new
DIN from dry atmospheric deposition. Atmospheric DIN fluxes from dry deposition presented
a low variability along the transect ($29 \pm 7 \mu\text{mol N m}^{-2} \text{ d}^{-1}$ at the short stations) and were
among the lowest previously measured in the Mediterranean environment, ranging from 38 to
575 240 $\mu\text{mol N m}^{-2} \text{ d}^{-1}$ (Desboeufs et al., in press). It has to be noted that the fluxes measured
during the PEACETIME cruise are representative of the open sea atmosphere while published
fluxes were measured at coastal sites where local/regional contamination contributes
significantly to the flux (Desboeufs, in press). Atmospheric deposition also delivers organic
matter (Djaoudi et al., 2017, Kanakidou et al., 2018), which is bioavailable for marine hprok
580 (Djaoudi et al., 2020). Dissolved organic nitrogen (DON) released from aerosols, not
determined here, can be estimated from previous studies. On average in the MS, DON
solubilized from aerosols represents 32%. (range19 to 42%) of the total dissolved N released
from dry deposition (Desboeufs, in press). Considering this mean, DON released from dry
deposition was estimated to range from 8 to 19 $\mu\text{mol N m}^{-2} \text{ d}^{-1}$ at the short duration stations.
585 The total dissolved N solubilized from dry deposition (inorganic measured +organic
estimated) would thus represent 14 to 121% of the hprokN demand. Because of the low
variability in DIN (and estimated DON) fluxes derived from dry deposition, the atmospheric
contribution was mainly driven by biogeochemical conditions and not by the variability of
atmospheric fluxes during the cruise (CV of Nprok N_{demand} and phyto N demand at the
590 short stations were 45% and 89%, respectively, and that of DIN flux 25%). However, the
calculated contribution can also be biased by the deposition velocity used to calculate DIN

solubilized from the dry deposition. Deposition velocity was set at 1 cm s⁻¹ for NO3 and 0.21 cm s⁻¹ for NH4. As NO3 was the dominant inorganic form released by dry deposition, it is clear that the choice of 1 cm s⁻¹ for NO3 influenced its contribution. This choice was 595 conditioned by the predominance of NO3 in the large mode of Mediterranean aerosols such as dust or sea salt particles (e.g., Bardouki et al., 2003). However, the deposition velocity of NO3 between fine and large particles could range from 0.6 to 2 cm sec⁻¹ in the Mediterranean aerosols (e.g. Sandroni et al., 2007). Even considering the lower value of 0.6 cm sec⁻¹ from the literature, the contribution of DIN from atmospheric dry deposition to hprokN demand 600 within the ML would still be significant (up to 72%).

4.2 Biogeochemical response after a wet deposition event – N and P budgets at FAST site

Rain events are more erratic than dry atmospheric deposition but represent on average much higher new nutrient fluxes to the MS surface waters on an annual basis, e.g. 84% of annual 605 atmospheric DIN fluxes in Corsica Island (Desboeufs et al., 2018). At the scale of the Mediterranean basin, the annual wet deposition of DIN was found to be 2-8 times higher than DIN from dry deposition (Markaki et al., 2010). Wet deposition also contributes significantly to DON atmospheric fluxes in the MS: For example at Frioul Island (Bay of Marseille, NW MS), total (wet + dry) DON atmospheric fluxes ranged between 7 and 367 µmol DON m⁻² 610 day⁻¹ and represented 41 ± 14% of the total atmospheric nitrogen flux (Djaoudi et al., 2018). In the Eastern MS (Lampedusa Island) DON atmospheric fluxes ranged between 1.5 and 250 µmol DON m⁻² day⁻¹ contributing to 25% of the total atmospheric nitrogen flux, respectively (Galletti et al., 2020). In both studies, bulk atmospheric fluxes of DON were positively 615 correlated with precipitation rates, indicating the preponderance of wet deposition over dry deposition.

At the FAST site, the maximum net variations of NO3 and DIP concentrations within the ML before/after the rainy period reached 1520-665 = +855 µmol N m⁻² for NO3 and 281-137 = +144 µmol P m⁻² for DIP (Table S2). In other terms, based on a mean MLD of 16 m, the net 620 observed increases in the ML were + 9 nM DIP and + 54 nM NO3. These net variations observed in the ML are higher than the calculated variation in stocks deduced from the N and P concentrations of this rain event (0.07 nM DIP and 21 nM NO3 concentrations increase over the whole ML (Table 3). This is still true when including all P or N chemical forms (particulate and soluble inorganic + organic fractions). For example the P concentration in the

625 ML would increase by ~0.68 nM. As described in the results section 3.4, the rains affecting
the FAST site were spatially patchy over a large area (~40-50 km radius around the R/V).
Thus, we consider that the biogeochemical impacts observed at FAST site were probably due
to a suite of atmospheric events rather than only the single event observed on board. It is also
possible that meso- and sub-mesoscale dynamics encountered at FAST site (Figs 5 and 12 in
630 Guieu et al., 2020) may have affected such cumulative impact.

Interestingly, a delay of about 19 h was observed in the maximum net accumulation within
the ML between DIP (FAST+1.05) and NO₃ (FAST+0.24). The DIN/DIP ratio in the rain
(1438) was much higher than the Redfield ratio. As the biological turnover of DIP in the MS
is rapid (from minutes to few hours, Talarmin et al., 2015), new DIP from rain might have
635 behaved differently than DIN. Two different mechanisms can explain this delay: (i) processes
linked to bypasses and luxury DIP uptake (storage of surplus P in hprok before a rapid
development of grazers (Flaten et al, 2005; Herut et al 2005, Thingstad et al., 2005) that are
later responsible for DIP regeneration) so that DIP net accumulation is delayed and/or (ii)
abiotic processes such as rapid desorption from large sinking particles followed by adsorption
640 of DIP onto submicronic iron oxides still in suspension as observed experimentally in Louis et
al. (2015).

The first proposed mechanism may be supported by the observed increase of BP, along with a
stable PP which suggests an immediate benefit of the new nutrients from rain by hprok rather
than phytoplankton. The so-called luxury DIP uptake by the competing organisms like hprok
645 is efficient (small cells with high surface/volume ratio and DIP kinetic uptake adapted to low
concentrations). It is of course difficult to quantify such *in situ* variations in comparison to
mesocosms/minicosms dust addition experiments, in which clearly heterotrophy is favoured
first (Marañón et al., 2010; Guieu et al., 2014b; Gazeau et al., 2021). Few attempts in the field
have confirmed these trends (Herut et al., 2005, Pulido-Villena et al., 2008) but, as stated in
650 the introduction, these studies lacked high frequency sampling.

The second proposed mechanism, the abiotic desorption/adsorption, is compatible with the
observed 19 h delay (Louis et al., 2015). Note that most of the estimates of such abiotic
processes are from dust addition experiments with contrasting results, some showing this
abiotic process of absorption/desorption while the particles are sinking (Louis et al., 2015),
655 and other not (Carbo et al., 2005) or showing it as negligible in batch experiments (Ridame et
al., 2003). It is possible that DIP adsorbed onto large particles rapidly sinks out of the ML,

and desorbs partly during its transit in the PDLb, where it could stay longer thanks to the pycnoclines barriers.

We made a tentative P budget between FAST+1.05 and FAST+2.11 where a net decrease of DIP ($-87 \mu\text{mol P m}^{-2}$) was observed in the ML. During this time, advective flux of DIP toward the PDLb was not detectable as DIP concentrations within the ML were always lower than within the PDLb (Pulido-Villena et al., 2021.). This indicated that the DIP was assimilated and/or transformed to DOP via biological processes, and/or adsorbed onto particles and then exported to PDLb by sedimentation. By integration of PP and BP over this period (34.5 and 660 19.7 mg C m⁻², respectively) and, by assuming that all the disappearing $87 \mu\text{mol DIP m}^{-2}$ would be consumed by hprok and phytoplankton, a C/P ratio reached in their biomass would be 52. Such C/P suggests that DIP was not limiting these organisms anymore. Indeed a 665 decrease of C/P quotas may highlight a switch from P to C limitation for heterotrophic bacteria (Godwin and Cotner, 2015) and from P to N limitation or increased growth rates for phytoplankton (Moreno and Martiny, 2018). Furthermore, as DIP is also recycled via alkaline phosphatase within the ML, we also consider another source of DIP via alkaline phosphatase activity, from which *in situ* activity (see Van Wambeke et al., 2021 for *in situ* estimates) 670 could release $139 \mu\text{mol DIP m}^{-2}$ during this period. Assuming also that DIP resulting from AP hydrolysis was fully assimilated for P biological needs, then C/P ratio would be 19. This low 675 ratio seems unrealistic for phytoplankton (Moreno and Martigny, 2018) as well as hprok, even growing in surplus C conditions (Makino et al., 2003; Lovdal et al., 2008; Godwin and Cotner, 2015).

Some of the P recycled or brought into the ML from atmospheric deposition has consequently 680 been exported below the ML. DIP is abiotically adsorbed on mineral dust particles (Louis et al., 2015), and constitute a source of export out of the ML while the particle sink. It is also possible that such sorbing process on dust particles enables the export of other P-containing organic molecules, for instance DOP or viruses produced following luxury DIP assimilation. Free viruses, richer in P than N relative to Hprok, could adsorb, like DOM, onto dust particles and constitute a P export source. Indeed, free viruses adsorb onto black carbon particles, 685 possibly reducing viral infection (Mari et al., 2019; Malits et al., 2015). However, particle quality is a determining factor for DOM or microbial attachment, and what has been shown for black carbon particles is not necessarily true for dust particles. For instance the addition of Saharan dust to marine coastal waters led to a negligible sorption of viruses to particles and increased abundance of free viruses (Pulido-Villena et al., 2014), possibly linked to an

690 enhancement of lytic cycles in the ML after relieving limitation (Pradeep Ram and Sime-Ngando, 2010).

We are aware of all the assumptions made here, including (i) conversion factors, (ii) *in situ* estimates of alkaline phosphatase, (iii) some missing DIP sources in the budget, such as the excretion of zooplankton estimated to amount to 22-37% of the phytoP demand at FAST site
695 (Feliú et al., 2020), iv) lack of knowledge on the different mechanisms linking P to dust particles, and (iv) considering the station as a 1D system. Nevertheless, all these results together suggest that both luxury consumption by Hprok and export via scavenging on mineral particles probably occurred simultaneously and could explain the observed variations of DIP in the ML.

700

For NO₃, and in contrast to the observations for DIP, we observed physical exchanges by advection between the ML and NDLb. A N budget within the ML during the period of net NO₃ decrease (between FAST+0.24, and FAST+2.11, Table S2), indicates a net loss of 1343 $\mu\text{mol N m}^{-2}$. For this period lasting 1.8 days, the time-integrated phytoN and hprokN demands
705 were 682 $\mu\text{mol N m}^{-2}$ and 378 $\mu\text{mol N m}^{-2}$, respectively, so that total biological demand in the ML was 1060 $\mu\text{mol N m}^{-2}$. During this period, the possible N sources used were net NO₃ decrease assumed to be consumption = 1343 $\mu\text{mol N m}^{-2}$ as well as N₂ fixation = 13 $\mu\text{mol N m}^{-2}$ and *in situ* aminopeptidase activity = 87 $\mu\text{mol N m}^{-2}$. In total, the possible source of N amounted to 1443 $\mu\text{mol N m}^{-2}$. Keeping in mind that the same potential caveats pointed to
710 DIP (see above) also apply for the calculation of N budget, the biological N demand appeared lower than the sources (difference \sim 380 $\mu\text{mol N m}^{-2}$). On the other hand, at FAST site, vertical advective fluxes of NO₃ from ML to NDLb were up to 337 $\mu\text{mol N m}^{-2} \text{ d}^{-1}$ (Fig. 4), i.e. \sim 600 $\mu\text{mol N m}^{-2}$ was lost from the ML over 1.8 days. From these two different approaches, exported NO₃ should range between 380 and 600 $\mu\text{mol N m}^{-2}$ over this period.
715 Thus, about 40% of the NO₃ accumulated in the ML after the rain was likely exported by vertical advection to the NDLb. Organisms present in the DCM could benefit of this input of new nutrients. Indeed, PP and abundances of all 4 phytoplankton groups (*Synechococcus*, *Prochlorococcus*, nano and picoeukaryotes) increased at the DCM after 24h and remained high for 2 days after the rain event (Fig. S3). The increase in abundances were higher for
720 prokaryotic phytoplankton abundances, as such organisms would likely benefit from their small size and their ability to use DON/DOP organic molecules (Yelton et al., 2016).

5. Conclusions

This study reports for the first time, in the context of an oceanographic cruise, simultaneous
725 sampling of atmospheric and ocean biogeochemical parameters to characterize the *in situ*
biogeochemical responses to atmospheric deposition within the ML. High-frequency
sampling, in particular at the FAST site, confirmed the transitory state of exchanges between
the ML and the NDLb. Even if dry deposition measured along the transect was homogeneous
and amongst the lowest observed in the MS, that input could represent up to 121% of the
730 hprokN demand. Furthermore, the signature of the dust wet deposition event on DIP and DIN
concentrations was clearly detected, considering both the local rain fluxes and the horizontal
oceanic mixing of water masses affected by the rain front.

Our results have shown the important role played by the ML in the biogeochemical and
735 physical processes responsible for transfers of nutrients between the atmosphere and the
nutrient depleted layer below. Thanks to the use of the LWCC technique and access to
nanomolar variations of NO₃ and DIP in repeated CTD casts, it was possible to demonstrate
the role of the ML and exchanges of NO₃ from the ML to the NDLb by vertical advection
when variations of MLD occurred simultaneously to transitory accumulation of NO₃ after a
deposition event. The time sequence occurring after a wet dust deposition event was
740 summarized as follows (Fig. 6) : accumulation of NO₃ in the ML, advection to NDLb, luxury
consumption of DIP by hprok and delayed peaks of DIP, decrease of primary production and
subsequent recovery after 2 days, mainly visible in the nutrient depleted layer. Dust
deposition triggers a complex and time-controlled trophic cascade within the microbial food
web. Our study shows the important role of intermittent, but strong abiotic effects such as
745 downwelling advective fluxes from the ML to the nutrient depleted layers. It will be
important to consider these aspects in biogeochemical budgets and models, especially when
climate and anthropogenic changes are predicted to increase aerosol deposition in the
Mediterranean Sea.

Data availability

750 Guieu et al., Biogeochemical dataset collected during the PEACETIME cruise. SEANOE.
<https://doi.org/10.17882/75747> (2020).

Author contribution

CG and KD designed the study. FVW measured ectoenzymatic activity and BP, AE
755 managed the TAA analysis and treatments, EP measured DIP with the LWCC technique,
CR measured nitrogen fixation, VT assisted in CTD operations and analyzed water
masses, JD sampled for DOC and flow cytometry, EM analyzed the primary production
data, FVW prepared the ms with contribution from all co-authors.

760 **Competing interests**

The authors declare that they have no conflict of interest.

Special issue statement

This article is part of the special issue ‘Atmospheric deposition in the low-nutrient–low-
765 chlorophyll (LNLC) ocean: effects on marine life today and in the future (ACP/BG inter-
journal SI)’. It is not associated with a conference.

Financial support

The project leading to this publication received funding from CNRS-INSU, IFREMER,
770 CEA, and Météo-France as part of the program MISTRALS coordinated by INSU (doi:
10.17600/17000300) and from the European FEDER fund under project no 1166-39417.
The research of EM was funded by the Spanish Ministry of Science, Innovation and
Universities through grant PGC2018-094553B-I00 (POLARIS).

775 **Acknowledgements.** This study is a contribution of the PEACETIME project
(<http://peacetimoproject.org>, last access 13/07/2021), a joint initiative of the MERMEX
and ChArMEx components. PEACETIME was endorsed as a process study by
GEOTRACES and is also a contribution to IMBER and SOLAS international programs.
The authors thank also many scientists & engineers for their assistance with
780 sampling/analyses: Samuel Albani for NO₃ nanomolar sampling and Maryline Montanes for
NO₃ with LWCC technique, Marc Garel, Sophie Guasco and Christian Tamburini for
ectoenzymatic activity, Ruth Flerus and Birthe Zancker for TAA, Joris Guittoneau and Sandra
Nunige for nutrients, Thierry Blasco for POC, Julia Uitz and Céline Dimier for TChl a
(analysed at the SAPIG HPLC analytical service at the IMEV, Villefranche), María Pérez
785 Lorenzo for primary production measurements, Philippe Catala for flow cytometry analyses,
Barbara Marie and Ingrid Obernosterer for DOC analyses and treatments, Sylvain Triquet and

Franck Fu for atmospheric particulate nitrogen and phosphorus and PEGASUS team for atmospheric sampling. Maurizio Ribera d'Alcala and a second anonymous reviewer helped much to improve this ms.

790

References

Aminot, A., and Kérouel, R. : Dosage automatique des nutriments dans les eaux marines, in: Méthodes d'analyses en milieu marin, edited by: IFREMER, Plouzané, 188 pp, ISBN no 978-2-7592-0023-8, 2007.

795 Bardouki, H., Liakakou, H., Economou, C., Sciare, J., Smolik, J., Zdimal, V., Eleftheriadis, K., Lazaridis, M., Dye, C., and Mihalopoulos, N.: Chemical composition of size resolved atmospheric aerosols in the eastern Mediterranean during summer and winter, *Atmos. Environ.*, 37, 195–208, 2003.

Bonnet, S., Grosso, O., and Moutin, T.: Planktonic dinitrogen fixation along a longitudinal gradient across the Mediterranean Sea during the stratified period (BOUM cruise), *Biogeosciences*, 8, 2257–2267, 2011.

800 Bonnet, S., Caffin, M., Berthelot, H., and Moutin, T.: Hot spot of N₂ fixation in the western tropical South Pacific pleads for a spatial decoupling between N2 fixation and denitrification, *PNAS letter*, doi: 10.1073/pnas.1619514114, 2017.

805 Caffin, M., Berthelot, H., Cornet-Barthaux, V., Barani, A., and Bonnet, S.: Transfer of diazotroph-derived nitrogen to the planktonic food web across gradients of N₂ fixation activity and diversity in the western tropical South Pacific Ocean, *Biogeosciences*, 15, 3795–3810, doi: 10.5194/bg-15-3795-2018, 2018.

Carbo, P., Krom, M. D., Homoky, W. B., Benning, L. G., and Herut, B.: Impact of 810 atmospheric deposition on N and P geochemistry in the southeastern Levantine basin, *Deep Sea Res. II*, 52, 3041–3053. doi: 10.1016/j.dsr2.2005.08.014, 2005.

Céa, B., Lefèvre, D., Chirurgien, L., Raimbault, P., Garcia, N., Charrière, B., Grégori, G., Ghiglione, J.-F., Barani, A., Lafont, M., and Van Wambeke, F.: An annual survey of bacterial production, respiration and ectoenzyme activity in coastal NW Mediterranean

815 waters: temperature and resource controls, Environ. Sci. Pollut. Res., doi:
10.1007/s11356-014-3500-9, 2014.

Christaki, U., Courties, C., Massana, R., Catala, P., Lebaron, P., Gasol, J. M., and Zubkov, M.: Optimized routine flow cytometric enumeration of heterotrophic flagellates using SYBR Green I, Limnol. Oceanogr. Methods, 9, doi: 10.4319/lom.2011.9.329, 2011.

820 Cullen, J. J., Franks, P. J., Karl, D. M., and Longhurst, A. L. A. N.: Physical influences on marine ecosystem dynamics. The sea, 12, 297-336, 2002.

de Boyer Montegut, C., Madec, G., Fisher, A. S., Lazar, A., and Jodicone, D.: Mixed layer depth over the global ocean: An examination of profile data and a profile-based climatology, Journal of Geophysical Research. Oceans, 109, C12003, doi:
825 10.1029/2004JC002378, 2004.

Delmont , T. O., Quince, C., Shaiber, A., Esen, Ö. C., Lee, S. T. M., Rappé, M. R., McLellan, S. L, Lücker, S. and Murat Eren, A.: Nitrogen-fixing populations of Planctomycetes and Proteobacteria are abundant in surface ocean metagenomes, Nature Microbiology, doi: 10.1038/s41564-018-0176-9, 2018.

830 Desboeufs, K.: Nutrients atmospheric deposition and variability, in: Atmospheric Chemistry and its Impacts in the Mediterranean Region (ChArMex book), Springer, in press.

Desboeufs, K., Bon Nguyen, E., Chevaillier, S., Triquet, S., and Dulac, F.: Fluxes and sources of nutrient and trace metal atmospheric deposition in the northwestern Mediterranean, Atmospheric Chemistry and Physics, 18, 14477–14492, doi: 10.5194/acp-18-14477-
835 2018, 2018.

Desboeufs, K., Fu, F., Bressac, M., Tovar-Sánchez, A., Triquet, S., Doussin, J-F., Giorio, C., Chazette, P., Disnaquet, J., Feron, A., Formenti, P., Maisonneuve, P., Rodriguez-Roméro, A., Wagener, T., Dulac, F., and Guieu, C.: Wet deposition in the remote western and central Mediterranean Sea: A source of trace metals to surface seawater?, Atmos. Phys. Chem., this special issue, in preparation.

840 Dittmar, T.H., Cherrier, J., and Ludwichowski, K.-U: The analysis of amino acids in seawater. In: Practical Guidelines for the Analysis of Seawater, edited by: Wurl, O., Boca Raton, FL: CRC-Press, 67–78, 2009.

D'Ortenzio, F., Iudicone, D., de Boyer Montegut, C., Testor, P., Antoine, D., Marullo, S.,
845 Santolieri, R., and Madec, G.: Seasonal variability of the mixed layer depth in the
Mediterranean Sea as derived from in situ profiles., *Geophysical Research Letters*, 32,
L12605, doi:10.1029/2005GL022463, 2005.

Djaoudi, K., Van Wambeke, F., Barani, A., Hélias-Nunige, S., Sempéré, R., and Pulido-
Villena, E.: Atmospheric fluxes of soluble organic C, N, and P to the Mediterranean
850 Sea: potential biogeochemical implications in the surface layer, *Progress in
Oceanography*, 163: 59-69, MERMEX special issue, doi:
10.1016/j.pocean.2017.07.008, 2017.

Djaoudi, K., Van Wambeke, F., Coppola, L., D'ortenzio, F., Helias-Nunige, S., Raimbault, P.,
Taillandier, V., Testor, P., Wagener, T., and Pulido-Villena, E.: Sensitive determination
855 of the dissolved phosphate pool for an improved resolution of its vertical variability in
the surface layer: New views in the P-depleted Mediterranean Sea, *Frontiers in Marine
Science*, vol 5, article 234, doi: 10.3389/fmars.2018.00234, 2018.

Djaoudi, K., Van Wambeke, F., Barani, A., Bhairy, N., Chevaillier, S., Desboeufs, K.,
Nunige, S., Labiad, M., Henry des Tureaux, T., Lefèvre, D., Nouara, A.,
860 Panagiotopoulos, C., Tedetti, M., and Pulido-Villena E.: Potential bioavailability of
organic matter from atmospheric particles to marine heterotrophic bacteria,
Biogeosciences, 17, 6271–6285, <https://doi.org/10.5194/bg-17-6271-2020>, 2020

Du, C., Liu, Z., Kao, S.-J., and Dai, M.: Diapycnal fluxes of nutrients in an oligotrophic
oceanic regime: The South China Sea, *Geophysical Research Letters*, 44, 11, 510–11,
865 518, doi: 10.1002/2017GL074921, 2017.

Feliú, G., Pagano, M., Hidalgo, P., and Carlotti, F.: Structure and function of epipelagic
mesozooplankton and their response to dust deposition events during the spring
PEACETIME cruise in the Mediterranean Sea, *Biogeosciences*, 17, 5417–5441,
<https://doi.org/10.5194/bg-17-5417-2020>, 2020.

870 Flaten, G. A., Skjoldal, E. F., Krom, M. D., Law, C. S., Mantoura, F. C., Pitta, P., Psarra, S.,
Tanaka, T., Tselepides, A., Woodward, E. M., Zohary, T., and Thingstad, T. F.: Studies
of the microbial P-cycle during a Lagrangian phosphate-addition experiment in the
Eastern Mediterranean, *Deep-Sea Res II*, 52, 2928–2943, 2005.

875 Fu, F., Desboeufs, K., Triquet, S., Doussin, J-F., Giorio, C., and Guieu, C.: Solubility and sources of trace metals associated with aerosols collected during cruise PEACETIME in the Mediterranean Sea, *Atmos. Phys. Chem.*, this special issue, in preparation.

880 Galletti, Y., Becagli, S., di Sarra, A., Gonnelli, M., Pulido-Villena, E., Sferlazzo, D. M., Traversi, R., Vestri, S., and Santinelli, C.: Atmospheric deposition of organic matter at a remote site in the Central Mediterranean Sea: implications for marine ecosystem, *Biogeosciences*, 17, 3669–3684, <https://doi.org/10.5194/bg-17-3669-2020>, 2020.

Gasol, J. M., and del Giorgio, P. A.: Using flow cytometry for counting natural planktonic bacteria and understanding the structure of planktonic bacterial communities, *Scientia Marina*, 64, 197–224, 2000.

885 Gazeau, F., Van Wambeke, F., Maraño, E., Pérez-Lorenzo, M., Alliouane, S., Stolpe, C., Blasco, T., Leblond, N., Zäncker B., Engel A., Marie, B., Dinasquet, J., and Guieu C.: Impact of dust addition on the metabolism of Mediterranean plankton communities and carbon export under present and future conditions of pH and temperature, *Biogeosciences Discuss.* [preprint], <https://doi.org/10.5194/bg-2021-20>, in review, 2021.

890 Godwin, C. M., and Cotner, J. B.: Aquatic heterotrophic bacteria have highly flexible phosphorus content and biomass stoichiometry, *the ISME Journal*, 9, 2324–2327, doi:10.1038/ismej.2015.34, 2015.

Guieu, C., and Ridame, C.: Impact of atmospheric deposition on marine chemistry and biogeochemistry, in: *Atmospheric Chemistry and its Impacts in the Mediterranean Region* (ChArMex book), Springer, in press.

900 Guieu, C., Dulac, F., Desboeufs, K., Wagener, T., Pulido-Villena, E., Grisoni, J.-M., Louis, J., Ridame, C., Blain, S., Brunet, C., Bon Nguyen, E., Tran, S., Labiad, M., and Dominici, J.-M.: Large clean mesocosms and simulated dust deposition: a new methodology to investigate responses of marine oligotrophic ecosystems to atmospheric inputs, *Biogeosciences*, 7, 2765–2784, doi: 10.5194/BG-7-2765-2010, 2010.

Guieu, C., Aumont, O., Paytan, A., Bopp, L., Law, C. S., Mahowald, N., Achterberg, E. P., Maraño, E., Salihoglu, B., Crise, A., Wagener, T., Herut, B., Desboeufs, K., Kanakidou, M., Olgun, N., Peters, F., Pulido-Villena, E., Tovar-Sanchez, A., and

905 Völker, C.: The significance of episodicity in atmospheric deposition to Low Nutrient Low Chlorophyll regions, *Global Biogeochem. Cycles*, 28, 1179–1198, doi:10.1002/2014GB004852, 2014a.

Guieu, C., Ridame, C., Pulido-Villena, E., Bressac, M., Desboeufs, K., and Dulac, F.: Impact of dust deposition on carbon budget: a tentative assessment from a mesocosm approach, *Biogeosciences*, 11, 5621–5635, doi: 10.5194/bg-11-5621-2014, 2014b.

910 Guieu, C., D'Ortenzio, F., Dulac, F., Taillandier, V., Doglioli, A., Petrenko, A., Barrillon, S., Mallet, M., Nabat, P., and Desboeufs, K.: Process studies at the air-sea interface after atmospheric deposition in the Mediterranean Sea: objectives and strategy of the PEACETIME oceanographic campaign (May–June 2017), *Biogeosciences*, 17, 1–23, 2020, doi: 10.5194/bg-17-1-2020.

915 Heimburger, A., Losno, R., Triquet, S., Dulac F., and Mahowald, N. M.: Direct measurements of atmospheric iron, cobalt and aluminium-derived dust deposition at Kerguelen Islands, *Global Biogeochem. Cy.*, 26, GB4016, doi:10.1029/2012GB004301, 2012.

Hersbach, H., Bell, B., Berrisford, P., Biavati, G., Horányi, A., Muñoz Sabater, J., Nicolas, J., Peubey, C., Radu, R., Rozum, I., Schepers, D., Simmons, A., Soci, C., Dee, D.,
920 Thépaut, J-N.: ERA5 hourly data on single levels from 1979 to present. Copernicus Climate Change Service (C3S) Climate Data Store (CDS). doi: 10.24381/cds.adbb2d47, 2018.

Herut, B., Zohary, T., Krom, M. D., Mantoura, R. F. C., Pitta, P., Psarra, S., Rassoulzadegan, F., Tanaka, T. and Thingstad, T. F.: Response of East Mediterranean surface water to
925 Saharan dust: On-board microcosm experiment and field observations, *Deep-Sea Research II* 52 (2005) 3024–3040, 2005.

Herut, B., Rahav, E., Tsagaraki, T. M., Giannakourou, A., Tsiola, A., Psarra, S., Lagaria, A., Papageorgiou, N., Mihalopoulos, N., Theodosi, C. N., Violaki, K., Stathopoulou, E., Scoullos, M., Krom, M. D., Stockdale, A., Shi, Z., Berman-Frank, I., Meador, T. B.,
930 Tanaka, T., and Paraskevi, P.: The potential impact of Saharan dust and polluted aerosols on microbial populations in the East Mediterranean Sea, an overview of a mesocosm experimental approach, *Front. Mar. Sci.*, 3, 226, doi: 10.3389/fmars.2016.00226, 2016.

935 Hoppe, H.-G., Ducklow, H., and Karrasch, B.: Evidence for dependency of bacterial growth
on enzymatic hydrolysis of particulate organic matter in the mesopelagic ocean, Mar.
Ecol. Prog. Ser., 93, 277–283, 1993.

Ibello, V., Cantoni, C., Cozzi, S., and Civitarese, G.: First basin-wide experimental results on
N2 fixation in the open Mediterranean Sea, Geophys. Res. Lett., 37, L03608,
doi:10.1029/2009GL041635, 2010.

940 Izquierdo, R., Benítez-Nelson, C. R., Masqué, P., Castillo, S., Alastuey, A., and Ávila, A.:
Atmospheric phosphorus deposition in a near-coastal rural site in the NE Iberian
Peninsula and its role in marine productivity, Atmos. Environ., 49, 361–370, doi:
10.1016/j.atmosenv.2011.11.007, 2012.

945 Jumars, P. A., Penry, D. L., Baross, J. A., Perry, M. A., and Frost, B. W.: Closing the
microbial loop : dissolved carbon pathway to heterotrophic bacteria from incomplete
ingestion, digestion and absorption in animals, Deep-Sea Research, 483–495, 1989.

Kamykowski, D., and Zentara, S. J.: Nitrate and silicic acid in the world ocean: Patterns and
processes, Mar. Ecol. Prog. Ser., 26, 47–59, 1985.

950 Kanakidou, M., Myriokefalitakis, S., and Tsigaridis, K.: Aerosols in atmospheric chemistry
and biogeochemical cycles of nutrients, Environ. Res. Lett., 13, 063004, doi:
10.1088/1748-9326/aabedb, 2018.

Kanakidou, M., Myriokefalitakis, S., and Tsagkaraki, M.: Atmospheric inputs of nutrients to
the Mediterranean Sea, Deep Sea Research Part II: Topical Studies in Oceanography,
171, 104606, doi: 10.1016/j.dsr2.2019.06.014, 2020.

955 Kirchman, D. L.: Leucine incorporation as a measure of biomass production by heterotrophic
bacteria, in: Handbook of methods in aquatic microbial ecology, edited by : Kemp, P.F.,
Sherr, B.F., Sherr, E.B., and Cole, J.J., Lewis, Boca Raton, 509-512, 1993.

960 Kouvarakis, G., Mihalopoulos, N., Tselepidis, T., and Stavrakakis, S.: On the importance of
atmospheric nitrogen inputs on the productivity of eastern Mediterranean, Global
Biogeochemical Cycles, 15, 805–818, doi:10.1029/2001GB001399, 2001.

Krom, M. D., Herut, B., and Mantoura, R. F. C.: Nutrient budget for the eastern Mediterranean: Implication for phosphorus limitation, *Limnol. Oceanogr.*, 49, 1582–1592, doi: 10.4319/lo.2004.49.5.1582, 2004.

965 Louis, J., Bressac, M., Pedrotti, M.-L., and Guieu, C.: Dissolved inorganic nitrogen and phosphorus dynamics in sea water following an artificial Saharan dust deposition event, *Frontiers Marine Sci.*, 2, article 27, doi: 10.3389/fmars.2015.00027, 2015.

970 Løvdal, T., Skjoldal, E. F., Heldal, M., Norland, S., and Thingstad, T. F.: Changes in Morphology and Elemental Composition of *Vibrio splendidus* Along a Gradient from Carbon-limited to Phosphate-limited Growth, *Microb. Ecol.*, 55, 152–161, doi: 10.1007/s00248-007-9262-x, 2008.

Makino, W., Cotner, J. B., Sterner, R. W., and Elser, J. J.: Are bacteria more like plants or animals? Growth rate and resource dependence of bacterial C : N : P stoichiometry, *Functional Ecology*, 17, 121–130, 2003.

975 Malits, A., Cattaneo, R., Sintes, E., Gasol, J. M., Herndl, G. J., and Weinbauer, M.: Potential impacts of black carbon on the marine microbial community, *Aquat Microb Ecol.*, 75, 27–42, doi: 10.3354/ame01742, 2015.

980 Marañón, E., Fernández, A., Mouriño-Carballedo, B., Martínez-García, S., Teira, E., Cermeño, P., Chouciño, P., Huete-Ortega, M., Fernández, E., Calvo-Díaz, A., Morán, X. A. G., Bode, A., Moreno-Ostos, E., Varela, M. M., Patey, M. D., and Achterberg, E. P.: Degree of oligotrophy controls the response of microbial plankton to Saharan dust, *Limnology and Oceanography*, 55, 2339–2352, 2010.

985 Marañón, E., Van Wambeke, F., Uitz, J., Boss, E. S., Dimier, C., Dinasquet, J., Angel, A., Haëntjens, N., Pérez-Lorenzo, M., Taillardier, V., and Zäncker, B.: Deep maxima of phytoplankton biomass, primary production and bacterial production in the Mediterranean Sea, *Biogeosciences*, 18, 1749–1767, doi:10.5194/bg-18-1749-2021, 2021.

990 Mari, X., Guinot, B., Chu, V. T., Brune, J., Lefebvre, J.-P., Pradeep Ram, A. S., Raimbault, P., Dittmar, T., and Niggemann, J.: Biogeochemical Impacts of a Black Carbon Wet Deposition Event in Halong Bay, Vietnam, *Front. Mar. Sci.*, 6, article 185, doi: 10.3389/fmars.2019.00185, 2019.

Marie, D., Simon, N., Guillou, L., Partensky, F., and Vaulot, D.: Flow Cytometry Analysis of Marine Picoplankton, in: *In Living Color: Protocols in Flow Cytometry and Cell Sorting*, edited by: Diamond, R. A., and Demaggio, S., Springer, Berlin, Heidelberg, 421–454, 2000.

995 Markaki, Z., Loyer-Pilot, M. D., Violaki, K., Benyahya, L., and Mihalopoulos, N.: Variability of atmospheric deposition of dissolved nitrogen and phosphorus in the Mediterranean and possible link to the anomalous seawater N/P ratio, *Marine Chemistry*, 120, 187–194, doi: 10.1016/j.marchem.2008.10.005, 2010.

1000 Martiny, A. C., Pham, C. T. A., Primeau, F. W., Vrugt, J. A., Moore, J. K., Levin, S. A., and Lomas, M. W.: Strong latitudinal patterns in the elemental ratios of marine plankton and organic matter, *Nature geosciences*, 6, 279–283, doi: 10.1038/ngeo1757, 2013.

Mermex Group.: Marine ecosystems' responses to climatic and anthropogenic forcings in the Mediterranean, *Progress in Oceanography*, 91, 97–166, doi: 10.1016/j.pocean.2011.02.003, 2011.

1005 Mescioglu E., Rahav E., Frada M.J., Rosenfeld S., Raveh O., Galletti Y., Santinelli C., Herut B., Paytan A.: Dust-associated airborne microbes affect primary and bacterial production rates, and eukaryote diversity, in the Northern Red Sea: A mesocosm approach. *Atmosphere*, 10, article 358, doi: 10.3390/atmos10070358, 2019.

1010 Moreno, A. R., and Martiny, A. C.: Ecological stoichiometry of ocean plankton, *Ann. Rev. Mar. Sci.*, 10, 43–69, 2018.

Nagata, T.: Carbon and Nitrogen content of natural planktonic bacteria, *Appl. Environ. Microbiol.*, 52, 28–32, 1986.

1015 Orsini, D., Ma, Y., Sullivan, A., Sierau, B., Baumann, K., and Weber, R.: Refinements to the Particle-Into-Liquid Sampler (PILS) for Ground and Airborne Measurements of Water Soluble Aerosol Composition, *Atmospheric Environment*, 37, 1243–1259, 2003.

Omand, M. M. and Mahadevan, A.: The shape of the oceanic nitracline, *Biogeosciences*, 12, 3273–3287, doi: 10.5194/bg-12-3273-2015, 2015.

Pradeep Ram, A. S., and Sime-Ngando, T.: Resources drive trade-off between viral lifestyles in the plankton: evidence from freshwater microbial microcosms, *Environ Microbiol*, 12, 467–479, doi: 10.1111/j.1462-2920.2009.02088.x, 2010.

Prieur, L., D'Ortenzio, F., Taillandier, V. and Testor, P.: Physical oceanography of the Ligurian sea. In: Migon C., Sciandra A. & Nival P. (eds.), the Mediterranean sea in the era of global change (volume 1), evidence from 30 years of multidisciplinary study of the Ligurian sea, ISTE Sci. Publ. LTD, 49–78. doi:10.1002/9781119706960.ch3, 2020.

Pujo-Pay, M., and Raimbault, P.: Improvements of the wet-oxidation procedure for simultaneous determination of particulate organic nitrogen and phosphorus collected on filters, *Mar. Ecol. Prog. Ser.*, 105, 203–207, 1994.

Pulido-Villena, E., Wagener, T., and Guieu, C.: Bacterial response to dust pulses in the western Mediterranean: Implications for carbon cycling in the oligotrophic ocean, *Global Biogeochem. Cycles*, 22, GB1020, doi:10.1029/2007GB003091, 2008.

Pulido-Villena, E., Rérolle, V., and Guieu, C.: Transient fertilizing effect of dust in P-deficient surface LNLC ocean. *Geophysical Research Letters*, 37, L01603, doi:10.1029/2009GL041415, 2010.

Pulido-Villena, E., Baudoux, A.-C., Obernosterer, I., Landa, M., Caparros, J., Catala, P., Georges, C., Harmand, J., and Guieu, C.: Microbial food web dynamics in response to a Saharan dust event: results from a mesocosm study in the oligotrophic Mediterranean Sea, *Biogeosciences*, 11, 337–371, 2014.

Pulido-Villena, E., Desboeufs, K., Djaoudi, K., Van Wambeke, F., Barrillon, S., Doglioli, A., Petrenko, A., Taillandier, V., Fu, F., Gaillard, T., Guasco, S., Nunige, S., Triquet, S., and Guieu, C.: Phosphorus cycling in the upper waters of the Mediterranean Sea (Peacetime cruise): relative contribution of external and internal sources, *Biogeosciences Discuss.*, [preprint], <https://doi.org/10.5194/bg-2021-94>, in review, 2021.

Rahav, E., Herut, B., Levi, A., Mulholland, M. R., and Berman-Frank, I.: Springtime contribution of dinitrogen fixation to primary production across the Mediterranean Sea. *Ocean Sci.* 9, 489–498. doi: 10.5194/os-9-489-2013, 2013a

1050 Rahav, E., Herut, B., Stambler, N., Bar-Zeev, E. Mulholland, M. R., and Berman-Frank, I.: Uncoupling between dinitrogen fixation and primary productivity in the eastern Mediterranean Sea, *J. Geophys. Res. Biogeosci.*, 118, 195–202, doi:10.1002/jgrg.20023, 2013b.

1055 Rahav, E., Paytan, A., Chien, C.-T., Ovadia, G., Katz, T., and Herut, B.: The Impact of Atmospheric Dry Deposition Associated Microbes on the Southeastern Mediterranean Sea Surface Water following an Intense Dust Storm, *Front. Mar. Sci.*, 3, 127, doi: 10.3389/fmars.2016.00127, 2016.

1060 Richon, C., Dutay, J. C., Dulac, F., Wang, R., Balkanski, Y., Nabat, P., Aumont, O., Desboeufs, K., Laurent, B., Guieu, C., Raimbault, P., and Beuvier, J.: Modeling the impacts of atmospheric deposition of nitrogen and desert dust-derived phosphorus on nutrients and biological budgets of the Mediterranean Sea, *Prog. Oceanogr.*, 163, 21–39, doi: 10.1016/j.pocean.2017.04.009, 2018.

Ridame, C., Moutin, T., and C. Guieu.: Does phosphate adsorption onto Saharan dust explain the unusual N/P ratio in the Mediterranean Sea? *Oceanologica Acta*, 26, 629–634, doi: 10.1016/S0399-1784(03)00061-6, 2003.

1065 Ridame, C., Le Moal, M., Guieu, C. Ternon, E., Biegala, I., L'Helguen, S., and Pujo-Pay, M.: Nutrient control of N₂ fixation in the oligotrophic Mediterranean Sea and the impact of Saharan dust events, *Biogeosciences*, 8, 2773–2783, doi:10.5194/bg-8-2773-2011, 2011.

Sala, M. M., Peters, F., Gasol, J. M., Pedros-Alio, C., Marrasse, C., and Vaque, D.: Seasonal and spatial variations in the nutrient limitation of bacterioplankton growth in the northwestern Mediterranean, *Aquat. Microb. Ecol.*, 27, 47–56, 2002.

1070 Sandroni, V., Raimbault, P., Migon, C., Garcia, N., and Gouze, E.: Dry atmospheric deposition and diazotrophy as sources of new nitrogen to northwestern Mediterranean oligotrophic surface waters, *Deep-Sea Res. I*, 54, 1859–1870, doi:10.1016/j.dsr.2007.08.004, 2007.

Taillardier, V., Prieur, L., D'Ortenzio, F., Ribera d'Alcala, M., and Pulido-Villena, E.: Profiling float observation of thermohaline staircases in the western Mediterranean Sea and impact on nutrient fluxes, *Biogeosciences*, 17, 3343–3366, 2020.

Talarmin A, Van Wambeke F., Lebaron P., and Moutin T.: Vertical partitioning of phosphate uptake among picoplankton groups in the low Pi Mediterranean Sea, *Biogeosciences*, 12: 1237–1247 doi:10.5194/bg-12-1237-2015, 2015.

1080 Tanaka, T., Thingstad, T. F., Christaki, U., Colombet, J., Cornet-Barthaux, V., Courties, C., Grattepanche, J.-D., Lagaria, A., Nedoma, J., Oriol, L., Psarra, S., Pujo-Pay, M., and Van Wambeke, F.: Lack of P-limitation of phytoplankton and heterotrophic prokaryotes in surface waters of three anticyclonic eddies in the stratified Mediterranean Sea, *Biogeosciences*, 8, 525–538, doi: 10.5194/bg-8-525-2011, 2011.

1085 Tovar-Sánchez, A., Rodríguez-Romero, A., Engel, A., Zäncker, B., Fu, F., Marañón, E., Pérez-Lorenzo, M., Bressac, M., Wagener, T., Triquet, S., Siour, G., Desboeufs, K., and Guieu, C.: Characterizing the surface microlayer in the Mediterranean Sea: trace metal concentrations and microbial plankton abundance, *Biogeosciences*, 17, 2349–2364, <https://doi.org/10.5194/bg-17-2349-2020>, 2020.

1090 Thingstad, T., Krom, M. D., Mantoura, F., Flaten, G., Groom, S., Herut, B., Kress, N., Law, C. S., Pasternak, A., Pitta, P., Psarra, S., Rassoulzadegan, F., Tanaka, T., Tselepides, A., Wassmann, P., Woodward, M., Riser, C., Zodiatis, G., and Zohary, T.: Nature of phosphorus limitation in the ultraoligotrophic eastern Mediterranean, *Science*, 309, 1068–1071, doi: 10.1126/science.1112632, 2005.

1095 Van Wambeke, F., Christaki, U., Giannakourou, A., Moutin, T., and Souvemerzoglou, K.: Longitudinal and vertical trends of bacterial limitation by phosphorus and carbon in the Mediterranean Sea, *Microb. Ecol.*, 43, 119–133, doi: 10.1007/s00248-001-0038-4, 2002.

1100 Van Wambeke, F., Gimenez, A., Duhamel, S., Dupouy, C., Lefevre, D., Pujo-Pay, M., and Moutin, T.: Dynamics and controls of heterotrophic prokaryotic production in the western tropical South Pacific Ocean: links with diazotrophic and photosynthetic activity, *Biogeosciences*, 15: 2669–2689, doi: 10.5194/bg-15-2669-2018, 2018.

1105 Van Wambeke, F., Pulido-Villena, E., Catala, P., Dinasquet, J., Djaoudi, K., Engel, A., Garel, M., Guasco, S., Marie, B., Nunige, S., Taillandier, V., Zäncker, B., and Tamburini, C.: Spatial patterns of ectoenzymatic kinetics in relation to biogeochemical properties in

the Mediterranean Sea and the concentration of the fluorogenic substrate used,
Biogeosciences, 18, 2301-2323, doi:10.5194/bg-18-2301-2021, 2021.

Yelton, A. P., Acinas, S. G., Sunagawa, S., Bork, P., Pedros-Alio, C., Chisholm, S. W.:
Global genetic capacity for mixotrophy in marine picocyanobacteria, ISME J 10:2946-
1110 2957, 2016.

Zhang, J.-Z., and Chi, J.: Automated analysis of nano-molar concentrations of phosphate in
natural waters with liquid waveguide, Environ. Sci. Technol., 36, 1048–1053, doi :
10.1021/es011094v, 2002.

1115 **Table 1.** Main biogeochemical features/trophic conditions during the PEACETIME cruise.
 For TYR, ION and FAST sites investigated over several days, means \pm sd are indicated.
 1120 ITCchl: Integrated total chlorophyll a (Chla + dvChla). IPP: Integrated particulate primary
 production; IPB: integrated heterotrophic prokaryotic production. Integrations from surface to
 200 m depth for all data expect IPP, integrated down to the depth of 1% Photosynthetically
 Active Radiation (PAR) level.

	sampling date	Lat. °N	Long. °E	Temp. at 5 m °C	Bottom depth m	DCM depth m	ITChl a mg chla m ⁻²	IPP mg C m ⁻² d ⁻¹	IPB mg C m ⁻² d ⁻¹
ST1	May 12	41°53.5	6°20	15.7	1580	49	35.0	284	51
ST2	May 13	40°30.36	6°43.78	17.0	2830	65	32.7	148	55
ST3	May 14	39°0.8.0	7°41.0	14.3	1404	83	23.2	140	77
ST4	May 15	37°59.0	7°58.6	19.0	2770	64	29.2	182	66
ST5	May 16	38°57.2	11°1.4	19.5	2366	77	30.5	148	51
TYR	May 17-20	39°20.4	12°35.56	19.6	3395	80 \pm 6	29 \pm 3	170 \pm 35	57 \pm 3
ST6	May 22	38°48.47	14°29.97	20.0	2275	80	18.7	142	62
ST7	May 24	36°39.5	18°09.3	20.6	3627	87	24.2	158	57
ION	May 25-28	35°29.1	19°47.77	20.6	3054	97 \pm 5	29 \pm 2	208 \pm 15	51 \pm 9
ST8	May 30	36°12.6	16°37.5	20.8	3314	94	31.6	206	71
ST9	June 2	38°08.1	5°50.5	21.2	2837	91	36.1	214	64
FAST	June 2-7 and 9	37°56.8	2°54.6	21.0	2775	79 \pm 8	34 \pm 8	211 \pm 57	92 \pm 11
ST10	June 8	37°27.58	1°34.0	21.6	2770	89	28.9	nd	96

1125 **Table 2.** N budget at the short stations within the surface mixed layer (ML). Integrated stocks (NO₃, $\mu\text{mol N m}^{-2}$) and fluxes (heterotrophic prokaryotic N demand (hprokN demand), phytoplankton N demand (phytoN demand), in situ leucine aminopeptidase hydrolysis fluxes (LAP), dry atmospheric deposition of NO₃ and NH₄ (all fluxes in $\mu\text{mol N m}^{-2} \text{ d}^{-1}$). Values presented as mean \pm sd. SD was calculated using propagation of errors: For hprokN demand triplicate measurements at each depth and a C/N ratio of 7.3 ± 1.6 ; for phytoN demand triplicate measurements of PP at each depth and a C/N ratio of 7 ± 1.4 ; for LAP the analytical 1130 TAA error and the V_m and K_m errors; for N₂fix the coefficient of variation was 10% for volumetric fluxes $> 0.1 \text{ nmole N l}^{-1} \text{ d}^{-1}$ and 20% for lower values. For dry deposition, sd is based on the variability of the NO₃ and NH₄ concentrations solubilized from aerosols during the occupation of the station (see methods section 2.2.1). MLD: mixed layer depth. na: not available because under LWCC detection limits.

1135

stations	MLD	NO ₃	biological fluxes				Dry deposition	
			phytoN demand	hprokN demand	LAP	N ₂ fixation	NO ₃	NH ₄
	m	$\mu\text{mol N m}^{-2}$	$\mu\text{mol N m}^{-2} \text{ d}^{-1}$					
ST1	21	na	1468 ± 325	184 ± 40	121 ± 28	14.6 ± 1.5	18.6 ± 1.4	1.5 ± 0.3
ST2	21	na	481 ± 161	163 ± 35	48 ± 24	10.7 ± 1.1	23.7 ± 2.2	4.1 ± 0.9
ST3	11	na	282 ± 82	126 ± 28	40 ± 17	7.8 ± 0.8	33.8 ± 3.6	4.7 ± 0.5
ST4	15	na	246 ± 80	132 ± 28	83 ± 20	10.7 ± 1.1	23.8 ± 2.9	6.3 ± 2.6
ST5	9	261 ± 22	112 ± 29	42 ± 9	17 ± 12	4.8 ± 0.5	27.0 ± 7.5	7.9 ± 1.8
ST6	18	162 ± 14	410 ± 116	204 ± 44	48 ± 24	9.1 ± 0.9	15.0 ± 0.6	9.3 ± 0.7
ST7	18	162 ± 14	226 ± 123	148 ± 33	83 ± 18	10.5 ± 1.1	23.6 ± 1.9	8.0 ± 1.2
ST8	14	911 ± 77	274 ± 66	130 ± 33	25 ± 8	4.3 ± 0.5	13.4 ± 1.7	3.8 ± 0.6
ST9	7	819 ± 70	259 ± 70	85 ± 22	21 ± 6	3.4 ± 0.4	27.4 ± 3.8	13.5 ± 0.8
ST10	19	2074 ± 176	495 ± 31	294 ± 64	42 ± 26	13.6 ± 1.4	23.9 ± 3.4	4.1 ± 0.4

1140 **Table 3.** Characteristics and nutrient fluxes estimated in the 2 rain samples collected during
the PEACETIME cruise at ION and FAST sites.

event	Rain ION	Rain FAST
Date and local time	29/05 05:08-6:00	05/06 02:36-3:04
Estimated precipitation (mm)	3.5 ± 1.2	5.7 ± 1.4
DIP Flux nmol P m ⁻²	663 ± 227	1146 ± 290
DOP Flux nmol P m ⁻²	974 ± 334	908 ± 230
POP fluxes nmol P m ⁻²	239 ± 82	8801 ± 2227
NO ₃ Flux $\mu\text{mol N m}^{-2}$	67 ± 22	341 ± 86
NH ₄ Flux $\mu\text{mol N m}^{-2}$	71 ± 24	208 ± 53
DIN Flux $\mu\text{mol N m}^{-2}$	138 ± 47	550 ± 139

Figure legends

1145 **Figure 1.** Nitrate (NO₃) aerosol concentration along the PEACETIME transect. The locations of two rain events are indicated by large black circles. Stations ST 1 to 4 were not sampled for nutrient analysis at a nanomolar level.

Figure 2. Representation of the mixed layer (ML), the bottom of the nitrate (NO₃) depleted layer (NDLb), delineated by the nitracline depth and the mixed layer depth (MLD).

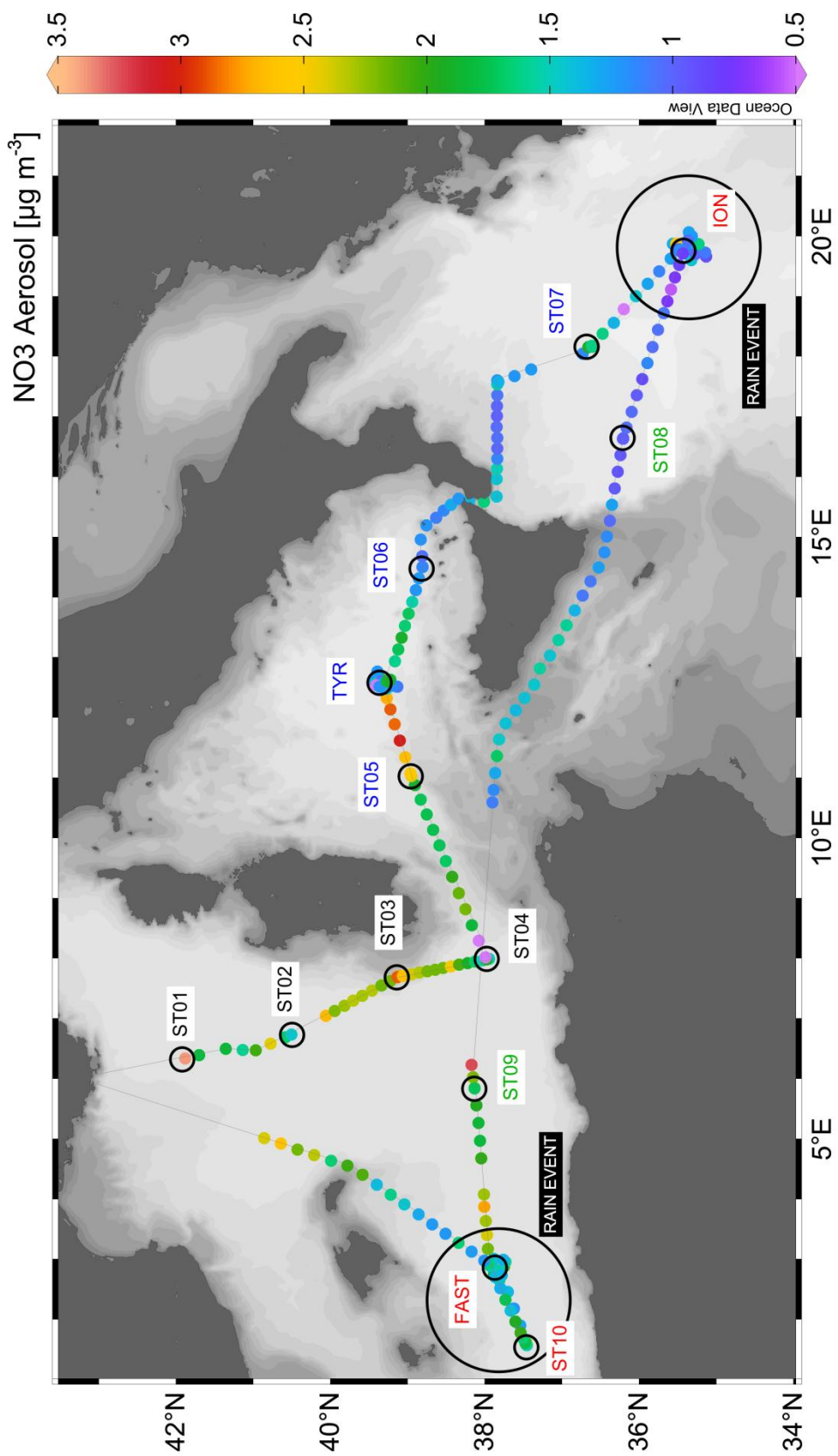
1150 **Figure 3.** a) Evolution of the wind speed during the PEACETIME cruise. The stations are indicated in yellow and dates in black. Vertical dotted lines delineate the beginning and the end of the ship's deployment at TYR, ION and FAST sites. The two rain events collected on board are indicated in solid vertical red arrows and surrounding observed rain events by horizontal dashed red arrows. b) 0-100 m vertical distribution of nitrate (NO₃) with depth. The MLD (in red) and nitracline (in brown) are indicated.

1155 **Figure 4.** Average concentration of nitrate (NO₃) in the ML and the NDLb, and NO₃ flux from the ML to NDLb. The stations have been classified into 4 types (1 in blue, 2 in green, 3 in yellow, 4 in red, see section Results and Table S1 for definitions). Error bars are indicated by standard deviation around average values for nitrate concentrations, and error propagation for the flux from ML to NDLb using a 0.5 m uncertainty in the MLD variation.

1160 **Figure 5.** Evolution within the ML of heterotrophic prokaryotic production (BP), particulate primary production (PP), heterotrophic prokaryotes (hprok) and *Synechococcus* (syn) abundances at the FAST site. The mixed layer depth is indicated by a red line.

1165 **Figure 6.** Synthetic view of biogeochemical processes and exchanges between the ML and NDLb at the FAST site before the rain and evolution after the rain.

Fig. 1



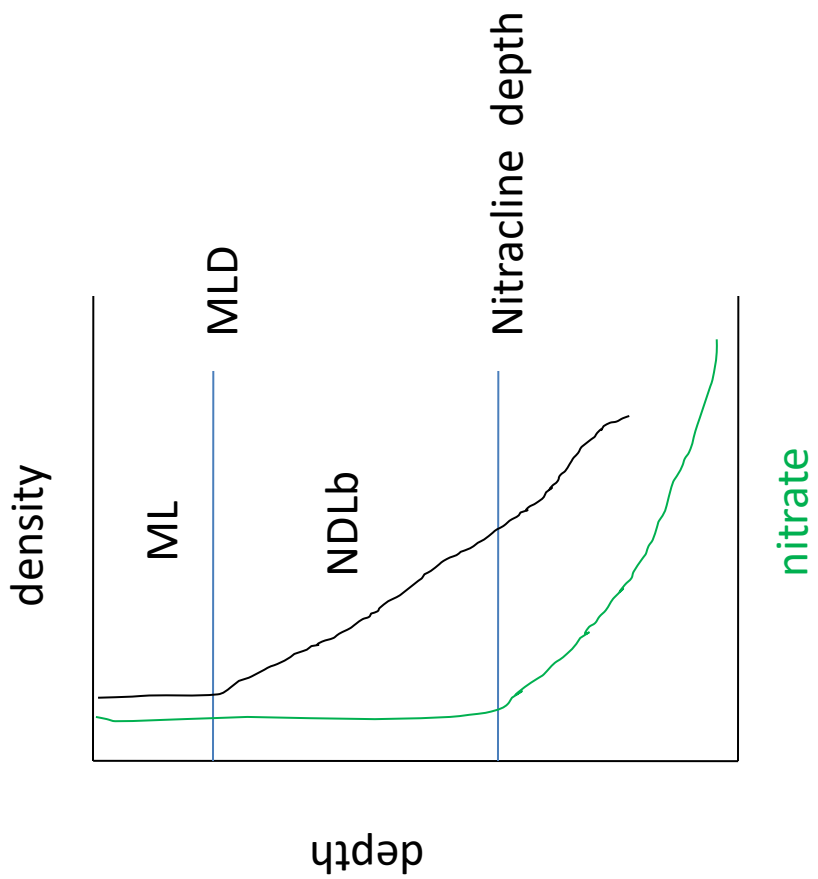


Fig.2

Fig. 3

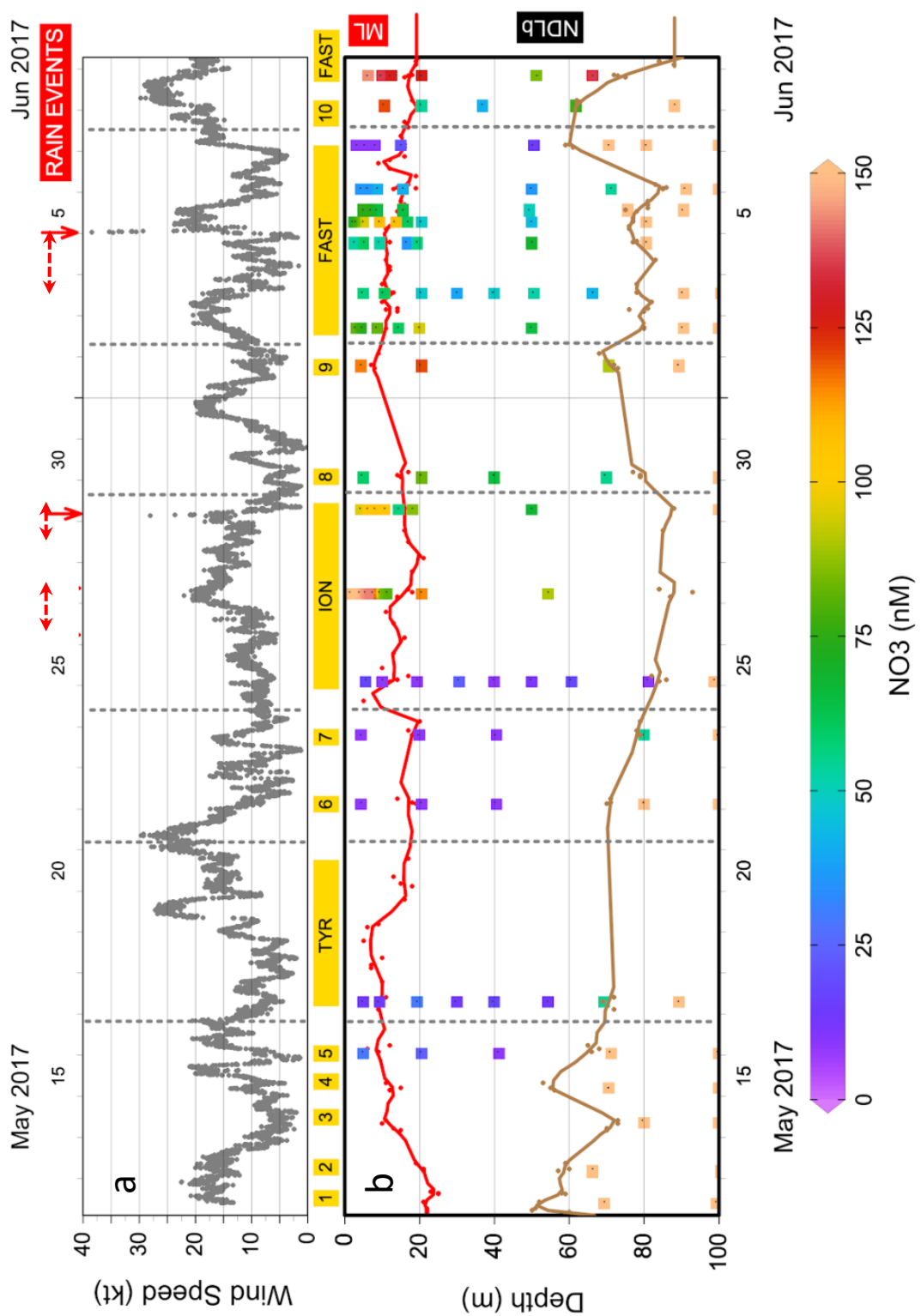


Fig. 4

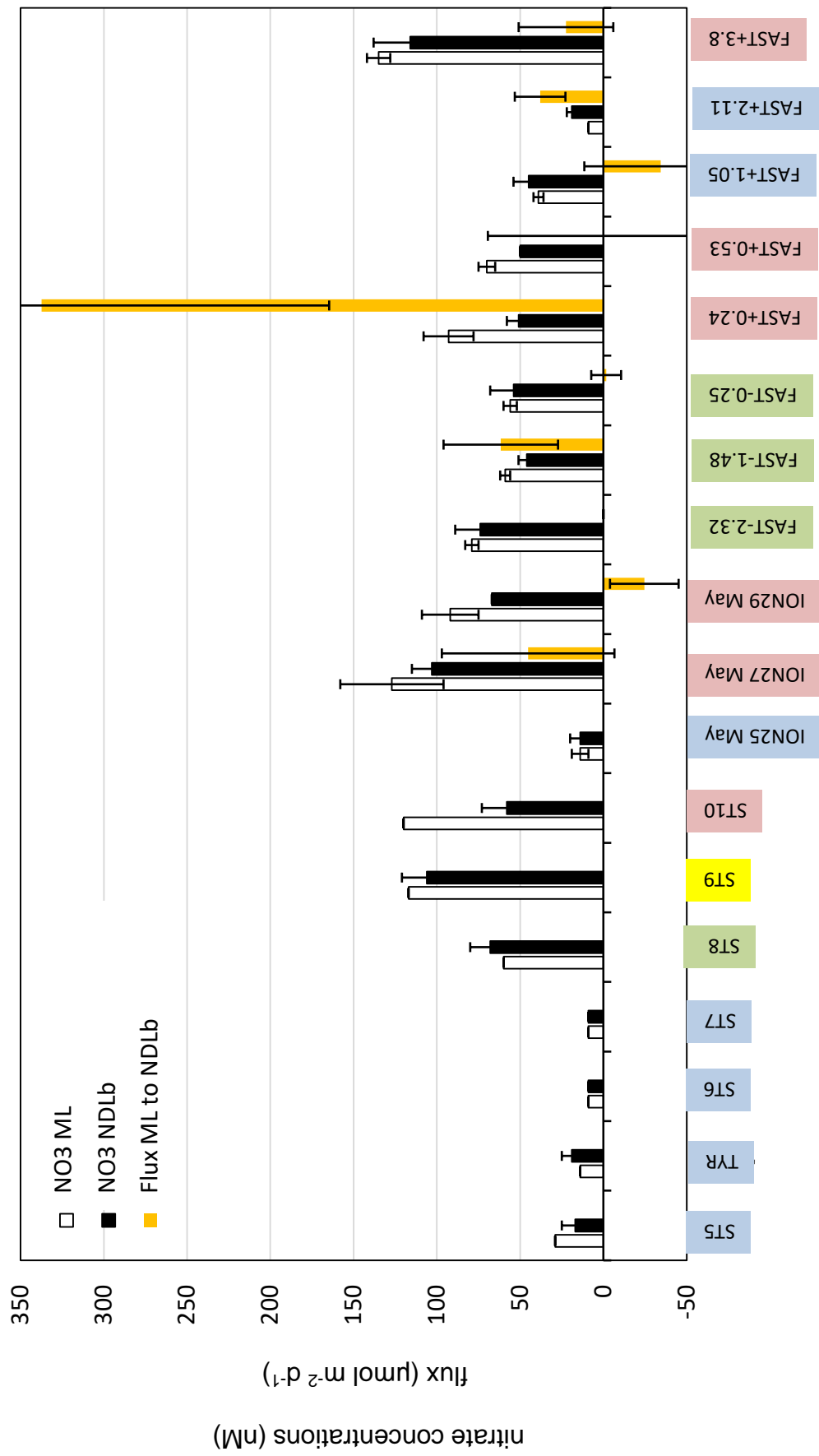


Fig. 5

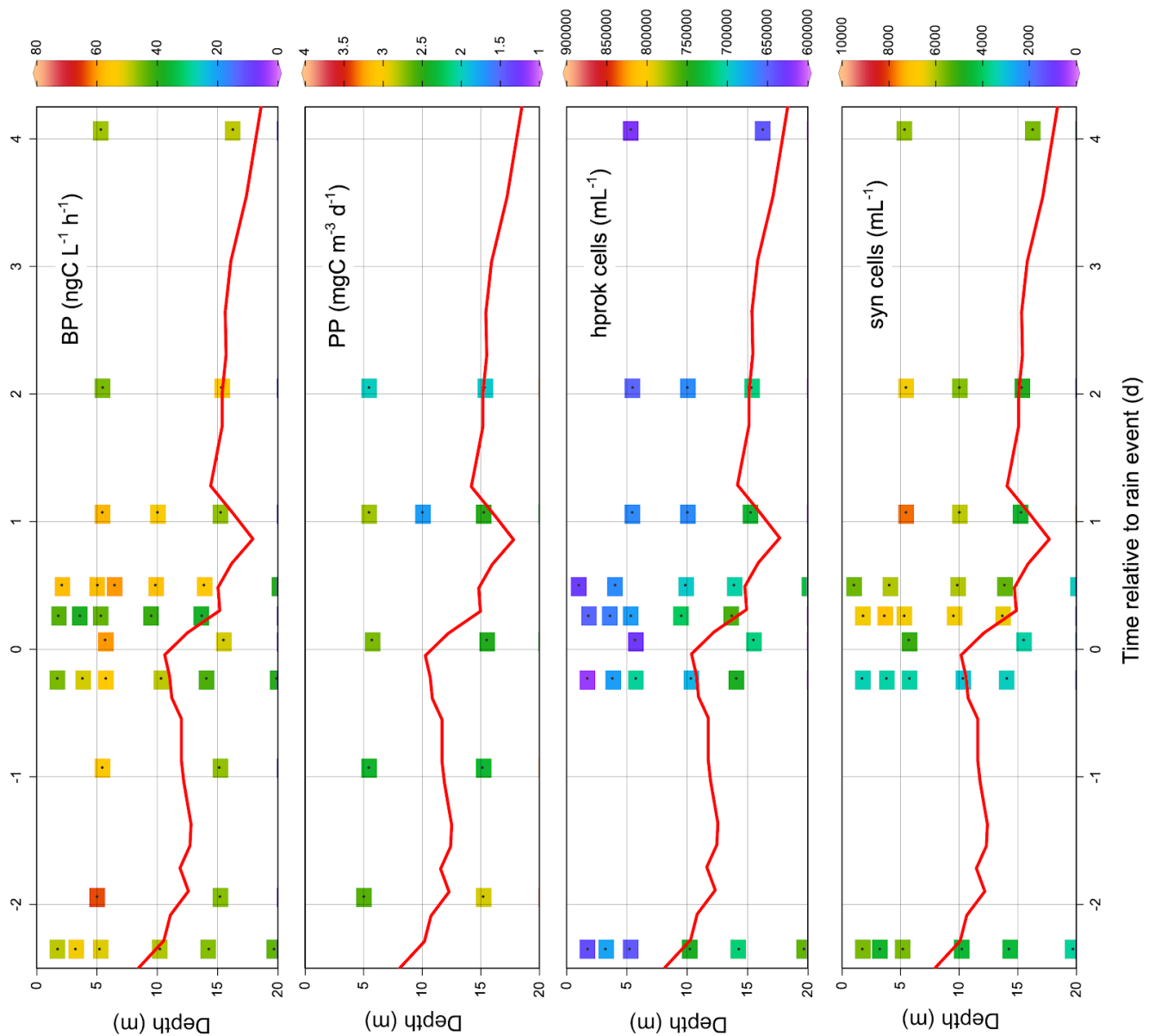


Fig. 6

